

Structures and geodynamics of the Mongolian tract of the Central Asian Orogenic Belt constrained by potential field analyses

Alexandra Guy, Schulmann Karel, Igor Soejono, N. Holzrichter, O. Lexa, Marc Munschy

▶ **To cite this version:**

Alexandra Guy, Schulmann Karel, Igor Soejono, N. Holzrichter, O. Lexa, et al.. Structures and geodynamics of the Mongolian tract of the Central Asian Orogenic Belt constrained by potential field analyses. Gondwana Research, 2021, 92, pp.26-53. 10.1016/j.gr.2020.11.016 . insu-03197629

HAL Id: insu-03197629
https://insu.hal.science/insu-03197629

Submitted on 14 Apr 2021

HAL is a multi-disciplinary open access archive for the deposit and dissemination of scientific research documents, whether they are published or not. The documents may come from teaching and research institutions in France or abroad, or from public or private research centers.

L'archive ouverte pluridisciplinaire **HAL**, est destinée au dépôt et à la diffusion de documents scientifiques de niveau recherche, publiés ou non, émanant des établissements d'enseignement et de recherche français ou étrangers, des laboratoires publics ou privés.

Journal Pre-proof



Structures and geodynamics of the Mongolian tract of the Central Asian Orogenic Belt constrained by potential field analyses

Alexandra Guy, K. Schulmann, I. Soejono, N. Holzrichter, O. Lexa, M. Munschy

PII: S1342-937X(20)30333-6

DOI: https://doi.org/10.1016/j.gr.2020.11.016

Reference: GR 2482

To appear in: *Gondwana Research*

Received date: 21 April 2020

Revised date: 6 November 2020

Accepted date: 18 November 2020

Please cite this article as: A. Guy, K. Schulmann, I. Soejono, et al., Structures and geodynamics of the Mongolian tract of the Central Asian Orogenic Belt constrained by potential field analyses, *Gondwana Research* (2020), https://doi.org/10.1016/j.gr.2020.11.016

This is a PDF file of an article that has undergone enhancements after acceptance, such as the addition of a cover page and metadata, and formatting for readability, but it is not yet the definitive version of record. This version will undergo additional copyediting, typesetting and review before it is published in its final form, but we are providing this version to give early visibility of the article. Please note that, during the production process, errors may be discovered which could affect the content, and all legal disclaimers that apply to the journal pertain.

© 2020 Published by Elsevier.

Journal Pre-proof

STRUCTURES AND GEODYNAMICS OF THE MONGOLIAN TRACT OF THE CENTRAL ASIAN OROGENIC BELT CONSTRAINED BY POTENTIAL FIELD ANALYSES

Alexandra Guy [a*], K. Schulmann [a, b], I. Soejono [a], N. Holzrichter [c], O. Lexa [d], M. Munschy [b]

[a] Centre for Lithospheric Research, Czech Geological Survey, Klárov 3, Prague, Czech Republic
[b] Institut de Physique du Globe de Strasbourg – CNRS UMR7516, Université de Strasbourg, France
[c] Institute of Geosciences, Christian-Albrechts-Universität, Kiel, Germany
[d] Institute of Petrology and Structural Geology, Charles University, Prague, Czech Republic

*corresponding author: alexandra.guy@gmail.com ; alexandra.guy@geology.cz

Abstract

A multidisciplinary approach integrating potential field analysis with geological and geochemical data provides new insights into the understanding of the crustal structure and evolution of the Mongolian collage. Magnetic and gravity data demonstrate the inconsistency between the geologically defined terranes and the geophysical domains in the southwestern part of the Mongolian collage. The combination of potential field analysis and modelling with whole rock geochemistry and isotopic mapping of Carboniferous–Permian granitoids indicates the presence of a homogeneous lower crust composed of a felsic to intermediate juvenile material beneath geophysically heterogeneous upper crust. This feature is interpreted as a result of a trench-directed lower crustal emplacement of an arc type crust underplating deformed Paleozoic oceanic crust. The potential field data also confirmed the occurrence of two orthogonal late Devonian and Permian–Triassic deformation upper crustal fabrics at the scale of the southwestern Mongolian collage. The prominent magnetic highs correspond to the tectono-metamorphic domains and magmatic provinces. The gravity anomalies highlight a periodicity of the signal correlating with alternating Permian–Triassic high and low strain zones, forming a zone of major deformation wrapping around the hinge of Mongolian orocline. The geometry and kinematics of dextral and sinistral transpressive faults are explained to result from the reactivation of Permian–Triassic deformation zones in the Cenozoic stress field.

KEYWORDS: Potential field analysis; Central Asian Orogenic Belt; crustal structure, geodynamics, geochemistry.

HIGHLIGHTS (85 CHARACTERS INCLUDING SPACES):

- Potential field data do not correlate with geologically defined terranes in the CAOB
- Geophysics determines two orthogonal supra-crustal Paleozoic and Mesozoic fabrics
- Geophysics and isotopic mapping identify a homogeneous lower crust

1. INTRODUCTION

Potential field data (namely magnetic and gravity data) suffer from the non-uniqueness of their interpretations as they primarily depend on the petrophysical properties (magnetic susceptibility and density) of rocks (Al-Chalabi, 1971; Saltus and Blakely, 2011). However, if combined with geological and structural analyses, they provide significant results when investigating orogens that are characterized by the amalgamation of contrasting geological units. This is because in these orogenic systems strong gravity and magnetic gradients result from the juxtaposition of different units with distinct densities and susceptibilities. The main objective of potential field data analysis is to enhance the locations and trends of these gradients by applying suitable filtering procedures in order to define the lateral distributions of crustal structures and their continuity in depth. These procedures include spectral techniques to distinguish the contribution to the geophysical field from sources located at different depths, data filtering to enhance the signals, multi-scale edge detection and also forward and inverse modelling of the gravity and magnetic data (Nabighian et al., 2005a, 2005b; and references therein). Potential field data analysis is thus widely used to study the architecture of both accretionary and collisional orogens such as the Tasmanides in Australia, the Northwestern Cordillera in America or the Variscan Belt in Europe (e.g. Aitken et al., 2009; Banka et al., 2002; Glen et al., 2007; Jones et al., 1983; Martínez-Catalán et al., 2012; Stewart and Betts, 2010; Wellman, 1988). Seismic data are usually regarded as a reliable tool providing more or less realistic images of lithological interfaces, large scale crustal structures and the topography of the Moho. However, except the seismic reflection experiments, they are not able to show the continuity of the structures as do the potential field methods.

Accretionary orogens result from the amalgamation of oceanic and continental units above long-lived Pacific type subduction systems. The accreted material originates from sequential additions of back-arcs, oceanic arcs, accretionary wedges, continental ribbons and oceanic floor stratigraphy sequences, which may be affected by recurrent magmatic recycling and crustal

differentiation leading to an extremely complex architecture (Cawood et al., 2009; Dhuime et al., 2012; Jahn et al., 2004). In addition, the formation of accretionary orogens can include or be followed by collisional processes leading to oroclinal folding, strike slip imbrications of accreted units and crustal flow processes (Guy et al., 2015; Schulmann and Paterson, 2011). The Central Asian Orogenic Belt (CAOB) is an archetypal accretionary orogen, the evolution of which started by the Proterozoic breakup of Rodinia and terminated with the formation of the eastern tract of the Pangea supercontinent in the Triassic (Fig. 1A). It is mainly composed of oceanic units and continental ribbons surrounded by the Gondwana-derived Tarim and North China cratons in the south and remnants of central Rodinia represented by the East European Craton and the Siberian Craton in the north (Wilhem et al., 2012 and references therein). The CAOB itself is formed by the Kipchak and the Tuva-Mongol arcs forming the Kazakhstan and Mongolian oroclines respectively, which resulted from the complex early Paleozoic accretionary, amalgamation and subduction processes (Sengör et al., 1993). Based on the differences in timing of accretion and the general structure of these two domains, Xiao et al. (2018) proposed to redefine these two oroclinal systems as the Kazakhstan and Mongolian collages (Figs. 1B and 2).

This review is an attempt to synthesize the potential field studies and modern geological data of the Mongolian collage and discuss the contribution of this approach to the understanding of the CAOB geodynamics. After presenting the geological background and the previous geophysical studies, we briefly present the potential field data and the applied filtering techniques. An integrated geophysical and geological approach is applied in southern Mongolia and northwestern China, and the significance and possible origin of the major anomalies are discussed in terms of lower crustal emplacement, location of the Devonian and Permian–Triassic deformation zones or main tectono-magmatic provinces. Finally, we discuss the geodynamic evolution of the whole system and the influence of the Cenozoic deformation on the final geophysical structure of the entire belt.

2. TECTONIC AND GEOLOGICAL SETTINGS OF THE CAOB: FROM REGIONAL TO LOCAL SCALE

After summarizing the tectonic context, the lithologies of the main tectonic zones, which compose southern Mongolia and northwestern China, are described. Synthetic lithostratigraphy columns constitute major constraints to interpret the possible sources of the different potential field signals and are presented here (Fig. 3).

2.1. Tectonic zonation

The Central Asian Orogenic Belt (CAOB) formed from the Proterozoic to early Mesozoic and resulted from two major phases: the accretionary phase from Neoproterozoic to Carboniferous, followed by the final N–S collisional phase in the Permian–Triassic involving the convergence of the Siberian Craton to the north with the Archean North China and Paleoproterozoic Tarim cratons to the south (e.g. Lehmann et al., 2010; Şengör et al, 1993; Wilhem et al., 2012; Windley et al., 2007). The CAOB is composed of different lithotectonic units such as Precambrian continental blocks, passive margins, oceanic domains, accretionary wedges, ophiolites, magmatic arcs and back-arc basins (Kröner et al., 2010 and reference therein). The Permian–Triassic collision was followed by late Jurassic–early Cretaceous continental scale extension affecting the east Asia (from the Baikal region to the north-east of eastern China) leading to the formation of NE–SW-oriented continental rift basins and metamorphic core complexes (Charles et al., 2012; Daoudene et al., 2009, 2012; Darby et al., 2004; Meng, 2003; Ren et al., 2002). Subsequently, it turned into an intracontinental orogen in the Cenozoic (Molnar and Tapponnier, 1975) accommodating the India-Eurasia convergence. The last event was related to the reactivation of all previous structures and the development of strike slip faults and thrusts in a general dextral transpressive regime (Calais et al., 2003; Cunningham et al., 2009).

Pioneering works of Badarch et al. (2002) and Windley et al. (2007) subdivided the Mongolian collage into a mosaic of numerous cratonal, arc, back-arc and accretionary wedge terranes due to their apparent heterogeneous lithological compositions. However, recent studies

(e.g., Guy et al., 2014b, 2020; Kröner et al., 2010) showed that these terranes can be grouped according to their age, geochemical, lithological, metamorphic and geophysical characteristics into lithotectonic zones (Fig. 2): The Mongol-Okhotsk Domain, the Mongolian Precambrian blocks, the Lake Zone, the Mongol Altai Accretionary Wedge, the East Junggar - Trans-Altai Domain and the South Gobi Zone. These zones are bounded by strike-slip faults, such as the Gobi-Tienshan, the East Gobi, the Char-Erqis, the Bogd and the Bulgan Fault zones (Buslov et al., 2001; Cunningham et al., 1996; Lamb et al., 1999). The Mongol-Okhotsk Domain (Fig. 3) in the north is a Silurian–Carboniferous embayment of the Paleo-Pacific Ocean presumably closed between Permian–early Cretaceous in a scissor-like manner (e.g. Cogné et al., 2005; Zonenshain et al., 1990). This oceanic domain consists of Silurian pelagic sediments and volcanic rocks, large Devonian–Carboniferous turbiditic deposits and remnants of Carboniferous ophiolitic sequences. The Mongolian Precambrian blocks, comprising the Barguzin, Tuva-Mongolia, Dzabkhan-Baydrag, Idermeg and Erguna blocks, (Fig. 1B) are composed of Paleoproterozoic–Grenvillian high-grade rocks and Neoproterozoic–Cambrian passive margin sequences (e.g. Wilhem et al., 2012 for review). The Lake Zone is a Neoproterozoic to early Cambrian accretionary wedge consisting of oceanic arcs, arc type volcanics and oceanic sediments, which were thrust over the Dzabkhan-Baydrag basement (Štípská et al., 2010; Zonenshain and Kuzmin, 1978). It is intruded by a Cambro–Ordovician calc-alkaline granitoids forming the giant Ikh-Mongol Arc (Janoušek et al., 2018). The Mongol Altai Accretionary Wedge (MAAW) stretches from Russia, through northwestern China to southern Mongolia and corresponds to a giant Cambro–Ordovician volcano-sedimentary accretionary wedge (Jiang et al., 2017; Soejono et al., 2018; Xiao et al., 2010) overlain by the late Silurian and early Devonian passive margin sequences (Zonenshain, 1973). This wedge was affected by the Devonian–Carboniferous magmatism, melting of deep crust and high-grade metamorphism (e.g. Broussolle et al., 2015; Jiang et al., 2016; Kozakov et al., 2002). The East Junggar in northwestern China and the Trans-Altai Zone in southern Mongolia form the East Junggar - Trans-Altai Domain (EJTA), which comprises early

Paleozoic intraoceanic ophiolitic sequences, covered by Silurian deep marine sediments, early Devonian basaltic and andesitic volcanics, and late Devonian to early Carboniferous volcanoclastic sediments (Lamb and Badarch, 2001; Ruzhentsev et al., 1985, 1992; Zonenshain, 1973). The Devonian and Carboniferous clastic material of the EJTA was partly sourced from the Ordovician MAAW. This similarity between the EJTA and MAAW uppermost crustal levels was further confirmed in northwestern China by comparison of the detrital zircon age populations (Guy et al., 2020 and reference therein). The Grenvillian age South Gobi Zone basement (Rojas-Agramontes et al., 2011) is covered by Ordovician–Silurian clastic sediments typical of a continental passive margin environment and Devonian–Carboniferous volcano-sedimentary and volcanic rocks.

2.2. Review of the relevant lithologies

The subdivision of the southwestern Mongolian collage into five major tectonic zones reflects the Paleozoic evolution of the region (Mossakovsky et al., 1993; Parfenov et al., 2003). The studied region can be characterized by the Mongolian Precambrian continental blocks in the north and the continental South Gobi Zone in the south, and a major oceanic domain in the centre represented by the EJTA, the MAAW and the Lake Zone (Janoušek et al., 2018; Kröner et al., 2010). In order to make possible the correlations between geological and potential field maps, we reviewed the geological information from the area of interest and produced simplified lithostratigraphic columns for each of the five lithotectonic zones (Fig. 3). The lithostratigraphic columns are compiled from previous studies (Broussolle et al., 2019; Guy et al., 2014b; Kröner et al., 2010; Markova 1975; Rauzer et al., 1987 and references below).

The Paleoproterozoic to early Paleozoic rocks of the Dzabkhan-Baydrag block consist of Paleoproterozoic to Grenvillian age tonalitic gneisses and metasedimentary rocks (Fig. 3) followed by the Neoproterozoic felsic to basaltic volcanic sequences (Bold et al., 2016; Levashova et al., 2011). The basement rocks are unconformably covered by Ediacaran to Lower Cambrian

limestones intercalated with dolomites, terrigenous sediments and calcareous sandstones (Khomentovsky and Gibsher, 1996; Vishnevskaya et al., 2015). The Neoproterozoic to Cambrian rocks of the Lake Zone (Fig. 3) are characterized by ophiolitic sequences (Buriánek et al., 2017; Zonenshain and Kuzmin, 1978), Cambrian eclogite facies mélange (Štípská et al., 2010), Devonian cover sequences (Kröner et al., 2010) and Carboniferous to Permian volcanic rocks. The MAAW (Fig. 3) consists essentially of sedimentary and volcano-sedimentary Cambro–Ordovician active margin sequences (Habahe Group in northwestern China and Tögrög Formation in Mongolia) and Upper Silurian to Lower Devonian passive margin carbonates and siliciclastic sediments (Kröner et al., 2010; Soejono et al., 2018). The rocks of the EJTA (Fig. 3) exposed to the south of the MAAW display ultramafic basement, covered by Silurian bedded cherts, Lower Devonian sequence of basalts, andesitic basalts and Upper Devonian volcano-sedimentary sequences typical for back-arc and intra-oceanic arc environments (Lamb and Badarch, 2001; Li P. et al., 2016; Novikov, 2013; Ruzhentsev et al., 1985). The higher part of the column is composed of Lower Carboniferous clastics followed by Upper Carboniferous–Lower Permian volcanism and Permian siliciclastic sediments. Finally, the rocks of the South Gobi Zone range from Neoproterozoic basement (outcrops located to the east of the South Gobi Zone) covered by continental margin Ordovician to Silurian sedimentary rocks (Johnson et al., 2008; Lehmann et al., 2010; Zonenshain, 1973) followed by Upper Devonian to Carboniferous thick volcanic sequences to Permian volcano-sedimentary strata. Mesozoic cover is heterogeneously developed in all zones and is characterized by Triassic to Lower Jurassic continental deposits.

3. PREVIOUS CRUSTAL SCALE GEOPHYSICAL STUDIES

The Mongolian collage does not have a dense geophysical data network as large data gaps exist over Mongolia and Russia and usually only coarse resolution grids are available for China. Below, an attempt is made to synthesize the previous large scale potential field studies over the Mongolian collage and adjacent areas. The gravity and magnetic data analyses often constitute secondary inputs to the studies and rarely concern "crustal scale" studies. However, during the

last decades, several works have mostly concentrated on the region of the Baikal rift system or targeted on the sedimentary basins (Fig. 4). The significant asymmetry of the Baikal rift system, the crustal structures and the contacts between the different tectonic zones in south Siberia and Central Mongolia were first revealed by gravity modelling based on gridded ground-based gravity data (Burov et al., 1994; Zorin et al., 1993, 1995) and confirmed later by forward and inverse gravity modelling combined with seismic analyses (Petit and Déverchère, 2006). South of the Baikal rift system, gravity and topography based models constrained by seismic tomography and receiver functions from the MOBAL profile identified the lithospheric structures between the Siberian Craton and the CAOB (Petit et al., 2002; 2008; Tiberi et al., 2008). With the help of GRACE satellite and terrestrial gravity data combined with magnetic data, Braitenberg and Ebbing (2009) investigated the late Permian–early Triassic basalt infill of the rift-graben structures of the West Siberian Basin. To the south, Dobretsov et al. (2017) attempted to characterize the geophysical structure of the Gorny Altai, but these authors used the free-air anomalies only, without correcting them for topographic effects (Fig. 4). At the scale of China, the airborne magnetic anomaly maps allow the assessment of the distribution of the igneous rocks including those which are not outcropping (Xiong et al., 2016). At a smaller scale, in northwestern China, gravity and magnetic mapping of the different Paleozoic arc systems and the distribution of magmatic intrusions in the Carboniferous strata were performed over the Junggar Basin (Li D. et al., 2016; Yushan et al., 2012). Joint gravity and magnetic data analyses were also used to map the polymetallic metallogenic belts to detect the most favorable areas for deposits in northwestern (An et al., 2018) and northeastern China (Wang et al., 2015). Tunini et al. (2016) integrated topographic, Bouguer anomaly, geoid, heat flow and seismic data as well as composition of mantle and crustal xenoliths along a 2D geophysical-petrological model in order to define the lithospheric structures and compositions. Finally, recent electromagnetic surveys along transects were performed in central Mongolia, which provide 3D crustal images (Comeau et al., 2018, 2020; Käufl et al., 2020).

4. POTENTIAL FIELD DATASETS USED IN THIS WORK

The datasets in this review come from different methods of acquisition (satellite, airborne and ground surveys) resulting in different resolution and depth sensitivity. In the section, we present the magnetic and gravity data over southern Mongolia and northwestern China at two different scales: (1) the large scale magnetic and gravity maps showing the continuity between southern Mongolia and northwestern China signal trends (Fig. 5); and (2) the regional potential field maps of southern Mongolia (Fig. 6) and northwestern China (Fig. 7).

4.1. Magnetic data and processing

Magnetic anomaly data over southern Mongolia were provided by Geophysical Exploration Technology (GETECH) in collaboration with the Mongolian Geological and Geophysical Exploration Company. They were digitized from maps of five airborne surveys and have a spatial resolution of 1 × 1 km. The reduction to the pole (RTP) was also applied to the data in order to remove the asymmetry of the magnetic anomalies and to center them over their sources. The procedure for merging these five airborne magnetic surveys is detailed in Guy et al. (2014b). The airborne magnetic map is superimposed on the Earth Magnetic Anomaly Grid (Maus et al., 2009) in order to fill the gaps (Fig. 6A)

Over northwestern China, the Earth Magnetic Anomaly Grid (EMAG2) available at a spatial resolution of 2 × 2 arc minute (~4 km) is used. It contains satellite and airborne measurements upward continued to 4 km above the geoid (Maus et al., 2009). To center the anomalies over their sources the RTP has been applied to the data according to the International Geomagnetic Reference Field (IGRF) of 2010 using 67.4° for inclination and 3.7° for declination and 57717 nT for magnitude of the regional magnetic field (Fig. 7A).

4.2. Gravity data and processing

Over southern Mongolia, the Bouguer anomaly data are derived from the DNSC08 free-air gravity model (Andersen and Knudsen, 2009) with a spatial resolution of 2 × 2 arc minute (~4

km) combining high-resolution topographic information with airborne and terrestrial gravity data. The computation of isostatic residual gravity anomalies was performed to the data in order to remove the long-wavelength signal (Fig. 6B; Guy et al., 2014b).

The Bouguer anomaly grid at a spatial resolution of 2.5 × 2.5 arc minute (~4.6 km) is available from the International Gravimetric Bureau. It derives from the Earth Global Model 08 (EGM08) and was used at the scale of northwestern China (Pavlis et al., 2012). The grid combines terrestrial, altimetry-derived, airborne gravity data and gravitational information derived from the topography over areas with lower resolution gravity data. In addition, as the Bouguer anomaly map shows long-wavelength information from the variation of the thickness of the crust and so conceals the shorter-wavelength responses from gravity sources located in the crust, the isostatic residual anomaly map has been computed. The computation consists in using the digital elevation model Earth2014 (Hirt and Rexer, 2015) and the Airy-Heiskanen compensation model (Heiskanen and Moritz, 1967) with the depth of the compensating root of 35 km at sea level in areas of no topography, a density contrast across the Moho of 330 kg/m^3 (Hinze et al., 2013), and a density of the reference crustal topography of 2670 kg/m^3 (Fig. 7B).

4.3. Potential field data filtering techniques

The gradients of magnetic and gravity anomalies are enhanced by performing suitable filtering procedures, which highlight the magnetic susceptibility and density contrasts. They enable the detection of significant crustal structures and the estimation of their continuity in depth. Thus, spectral analysis combined with matched filtering (pseudodepth slicing technique based on the analysis of the Fourier power spectrum) relies on the ability to deconvolve the signal into sets of sinusoids, where different wavelengths are linked to the different sources in depth (Phillips, 2001; Spector and Grant, 1970; Syberg, 1972). This technique helps to show the lateral variations of densities and magnetic susceptibilities within the corresponding depth layer and thus reveals the continuity of the major anomalies with depth. The tilt angle is computed to

enhance the gradients, extract the interpreted lineaments and analyze their trends. It deals with the ratio of the vertical to the total horizontal derivatives. As it is relatively insensitive to the depth of the source, this technique resolves shallow and deep sources equally well (Miller and Singh, 1994; Verduzco et al., 2004).

5. ANALYSIS AND INTERPRETATION OF MAGNETIC AND GRAVITY ANOMALIES

The following section first reviews and compares regional distribution of magnetic and gravity anomalies with geological data in two critical regions of the CAOB represented by southern Mongolia and northwestern China. Finally, we examine the geophysical and isotopic signature of the lower crust in both regions together.

5.1. Geophysical anomalies correlated to geological structures in southern Mongolia

Guy et al. (2014b, 2015) and Comeau et al. (2020) used the lack of systematic correspondence between the geophysical domains and the previously geologically defined major terranes to invalidate the existence of suspect terranes in southern Mongolia. In addition, the potential field analysis did not reveal any prominent deep-seated discontinuity which could be attributed to suture zones. Instead, at the scale of southern Mongolia, the magnetic map (Figs. 8A) shows a clear coincidence between large scale magnetic highs and early Permian volcanic and magmatic provinces, defined by Kovalenko et al. (2006) and Yarmolyuk et al. (2013) as crustal scale linear rift zones associated with major asthenospheric upwelling. These magnetic structures sometimes coincide with boundaries of tectonic zones but more often are clearly discontinuous with them (Fig. 8A). Importantly, the analysis of the isostatic residual gravity anomaly map revealed a periodic alternation of linear gravity highs and lows over the whole southern Mongolia (Figs. 8B and 9C). The magnetic and gravity highs observed in the Cretaceous and Cenozoic basins most probably correspond to basement magnetic and density sources which can be interpreted as the continuation of the Paleozoic outcrops surrounding the basins.

Previous studies of Guy et al. (2014b, 2015) demonstrated the link between Paleozoic and Mesozoic deformation fabrics of individual units forming the Mongolian collage and the magnetic and gravity lineaments. The structural analyses determined three types of deformation structures developed in southern Mongolia (Fig. 9D; Guy et al., 2014a; Lehmann et al., 2010): (1) the early Devonian S1 metamorphic schistosity developed mainly in the MAAW and to a lesser degree in the EJTA (2) the late Devonian–early Carboniferous N–S trending upright F2 folds and mantled gneiss domes in the MAAW and N–S striking thrust of intra-oceanic ophiolite sheets in the EJTA and the South Gobi Zone; (3) the ubiquitous crustal scale Permian–Triassic NW–SE upright folds and up to twenty kilometer wide deformation zones periodically reworking the Mongolian basement (e.g. Edel et al., 2014; Guy et al., 2014a; Lehmann et al., 2010). Two principal groups of magnetic and gravity lineaments could be distinguished in southern Mongolia (Fig. 9 A and B): (1) the NE–SW-oriented lineaments; and (2) the dominant NW–SE lineaments; and minor NNE–SSW-trended lineaments. The first group of lineaments occurs mainly in the western part of southern Mongolia and globally coincides with the Permian–Triassic structures and also with the Cenozoic ranges that were interpreted as the network of restraining bends by Cunningham (2013). On the other hand, less important NE–SW trending lineaments are mostly located in the eastern part of southern Mongolia and correspond to the trend of Cretaceous extensional fabrics and the discontinuities truncating the E–W trending linear gravity and magnetic highs. These discontinuous zones spatially, geometrically and kinematically coincide with the East Gobi sinistral strike-slip zones (Fig. 2). Finally, the NNE–SSW-trending short lineaments occur mainly in the western part of southern Mongolia and are visible only on local gravity anomaly map (Hanžl et al., 2020). They correspond to the remnants of late Devonian–early Carboniferous deformation fabrics.

The comparison of the magnetic and gravity lineaments with the regional geology (Figs. 8 and 9; Guy et al., 2014a; Lehmann et al., 2010) shows that: (1) the large scale magnetic highs correspond to high K calc-alkaline to alkaline magmatic provinces of Permian to Triassic age and

(2) the linear high frequency gravity and magnetic highs coincide with periodically alternating high-strain deformation zones characterized by subvertical fabrics and the occurrences of exhumed ultramafic basement. These zones were attributed to the NNE–SSW Permian–Triassic shortening event associated to a large-scale E–W realignment of all geological structures in southern Mongolia (Guy et al., 2014a). In contrast, magnetic and gravity lows correspond to the zones of weak Permian–Triassic deformation that are characterized by sub-horizontal fabrics and intermontane basins filled by Mesozoic and Cenozoic sediments.

5.2 Geophysical anomalies correlated to geological structures in northwestern China

Broussolle et al. (2019) suggested that the complex structure of the northwestern Chinese MAAW did not originate by amalgamation of suspect terranes, as proposed by previous studies (Windley et al., 2002; Xiao et al., 2004), but by polyphase metamorphic and magmatic reworking of a Cambro–Ordovician accretionary sedimentary wedge. The analyses of the magnetic and gravity anomaly maps support this suggestion as the geological terranes do not correspond with the geophysical domains. The correlation of potential field data with the geological map shows that magnetic and gravity lows mostly correspond to the metasedimentary sequence of the Ordovician Habahe Group and to the Mesozoic sedimentary basins (Figs. 10 and 11). In contrast, the Devonian magmatic province in the NE of northwestern Chinese MAAW correlates with intermediate to low magnetic signals and gravity highs. These geophysical characteristics can be related to the metamorphism and melting of Ordovician metagreywackes which produced hornblende bearing S-type granitoids (Jiang et al., 2016; Huang et al., 2020) characterized by a large amount of paramagnetic phases in granitoids (Bouchez, 2000) and high density anhydrous minerals in metamorphic rocks (Smithson, 1971). The potential field signals of the EJTA broadly display magnetic and gravity highs of low frequency in the north, and magnetic and gravity lows in the south, where the sedimentary cover is thicker (Fig. 7A). This feature indicates the continuation of a high density and high magnetic susceptibility Paleozoic basement beneath the Mesozoic sedimentary cover of the Junggar Basin.

As in Mongolia, the geophysical study of Guy et al. (2020) shows that the magnetic and gravity anomalies correlate with the Paleozoic and Mesozoic deformation fabrics. There are three important deformation fabrics developed in the northwestern Chinese MAAW and adjacent EJTA basement (Broussolle et al., 2019; Jiang et al., 2015, 2019; Zhang et al., 2015) (Fig. 11C): (1) an early to mid-Devonian regional sub-horizontal fabric affecting the whole crustal pile manifested by migmatitic layering developed in the orogenic lower crust, sub-horizontal sheets of S-type granitoids intruding Barrovian schists of the orogenic middle crust and sedimentary basins and volcanic extrusions in the orogenic upper crust (Jiang et al., 2016; Zhang et al., 2015); (2) large late Devonian NE–SW upright F2 folds associated with the formation of crustal scale gneiss domes exhuming the orogenic lower crust (Jiang et al., 2015); and (3) early Permian NW–SE trending upright folds and vertical high-strain zones locally associated with a partial melting and the intrusions of alkaline granitic bodies (Briggs et al., 2007; Li P. et al., 2017). The most important zone of Permian deformation occurs in the central part of the northwestern Chinese MAAW, where it is associated with the extrusion of a partially molten crust and (U)HT granulites and the intrusions of Permian gabbros and granitoids along a NW–SE trending tabular vertical zone (Broussolle et al., 2018; Jiang et al., 2019).

The early Devonian melting event is recorded only by large scale gravity high developed in the NW part of the MAAW (Fig. 11C). This anomaly was attributed to the existence of a dense granulitic residue beneath the crustal scale composite migmatite-magmatite dome that was constrained by both thermodynamic and gravity modelling (Jiang et al., 2016). Three principal sets of anomalies can be correlated to the deformation fabrics detected in the MAAW and EJTA (Figs. 10, 11 B and C): (1) the NW–SE-oriented mainly magnetic anomalies; (2) the NE–SW trending dominantly gravity anomalies; and (3) the N–S trending less important gravity and magnetic lineaments. Figures 10A and 11B show that the NW–SE magnetic lineaments match with the Permian and granulite facies deformation zone, the magmatism affecting the central part, the southern parts of the MAAW, and the Zhaheba ophiolite belt in the EJTA. Therefore,

we interpret these anomalies as a result of the Permian deformation, metamorphism and magmatism. Contrarily, Figures 10B and 11B shows that the NE–SW gravity lineaments match essentially with orientation of the late Devonian folds and gneiss domes developed in the central and northern part of the northwestern Chinese MAAW. Similar lineaments are also developed in the EJTA and were interpreted also as a result of the Devonian deformation (Guy et al., 2020).

In conclusion, the NE–SW oriented gravity lineaments coinciding with the late Devonian-Carboniferous deformation fabrics correspond to the N–S trending structures in southern Mongolia, which reflect general E–W shortening there. In the Chinese sector, these deformation fabrics were rotated to NE–SW position along the hinge of the Mongolian orocline in a manner described by Edel et al. (2014) and Guy et al. (2020). Both gravity and magnetic NW–SE oriented geophysical lineaments subparallel to the Permian orogenic fabrics in northwestern China correspond to similar large scale E–W trending Permian fabrics observed in southern Mongolia (Guy et al., 2020). Finally, the N–S trending lineaments which are clustered around the sub-parallel dextral strike-slip Fuyun Fault (Fig. 7) may correspond to Cenozoic fault network as defined by Cunningham (2013).

5.3. Contrasting geophysical signature of the upper and lower crust in southern Mongolia and northwestern China

In southern Mongolia, the comparison of the isostatic residual anomaly map with the regional Bouguer gravity map reveals regularly spaced gravity highs (Fig. 12A), which spatially correlate to high-strain zones of Permian-Triassic age (Guy et al., 2014b). The filtering of these short wavelength gravity highs from the upper to deep crusts indicates that the high-strain zones are rooted at ca. 20 km (Fig. 12D). The regional Bouguer anomaly map also reveals long wavelengths with relatively low amplitude around 45 mGal in the EJTA and the MAAW, and intermediate to high gravity signals in the South Gobi Zone and in the eastern part of the map (Fig. 12A). These observed changes of the gravity signal cannot be related to the variation of the crustal thickness because previous seismic experiments determined a flat topography of the

Moho underneath southern Mongolia (Mordvinova et al., 2007; Mordvinova and Artemyev, 2010; Teng et al., 2013; Zhang et al., 2014). Moreover, the upper and deep crustal gravity maps do not display a strong and continuous positive gravity anomaly over the supposed boundary separating the MAAW and the EJTA (called the Bulgan Fault in southwestern Mongolia). Therefore, the gravity analysis points towards a lack of deep crustal discontinuities between a geophysically heterogeneous upper crust and a lower crust beneath the MAAW and the EJTA. This discrepancy was further tested by means of forward magnetic and gravity modelling that was performed along a NE–SW cross-section perpendicular to the roughly E–W trending high-strain zones (Fig. 12D) in the MAAW, EJTA and South Gobi Zone (Guy et al., 2015). The constraints applied to the modeled profile are: (1) the lithostratigraphy and structural data gathered along geological cross-sections parallel to the geophysical profile (Guy et al., 2014a); (2) a flat Moho topography around 45 km established by the seismic studies (Mordvinova et al., 2007; Mordvinova and Artemyev, 2010; Teng et al., 2013; Zhang et al., 2014); and (3) the density and magnetic susceptibility values assigned according to the characteristic lithologies of individual tectonic zones (Clark and Emerson, 1991; Telford et al., 1990). The typical view of the three layered crust (Christensen and Mooney, 1995), the density values increasing with depth (Rudnick and Fountain, 1995) and the main geological boundaries at the surface were the starting point of this model. However, such a standard configuration could be maintained only for the South Gobi Zone. For the EJTA, the upper and middle crusts show the occurence of vertical tabular bodies deeply rooted in the crust up to ca. 20 km coinciding with the location of the Permian–Triassic high-strain zones (Fig. 12B, C and D). Guy et al., (2014a) shown that these high strain zones correspond to highly shortened Permo-Triassic synforms cored by Devonian ultramafic rocks and Devonian volcanic and volcano-sedimentary sequences imbricated during late Devonian–early Carboniferous orogeny (Zonenshain, 1973). In contrast, an intermediate density value of 2730 kg/m^3 was assigned to the MAAW and the EJTA lower crust. This density was proposed on the basis of isotopic mapping and geochemistry of Late Carboniferous and Permian granitoids

(Guy et al., 2014a), intermediate and felsic xenoliths trapped in tertiary volcanic rocks (Barry et al., 2003) and thermodynamic density modelling of intermediate granulite (Guy et al., 2015). Moreover, the magnetic signal along the modelling profile displays high frequency magnetic anomalies over the high strain zones, which coincide with the location of lenses of ultramafic rocks and mafic volcanic rocks in the Permian–Triassic highly shortened synforms in the Gurvansaykhan, Dzolen and Noyon ranges, respectively (Fig. 12 B, C and D). High frequency magnetic anomalies between the high-strain zones correlate with granitoids located in the low-strain zones.

In northwestern China, the comparison of the gravity signal of shallow and deep crust (Fig. 13A) shows a discrepancy. Here, a long wavelength gravity high can be observed in the southern MAAW and EJTA deep crust, which may indicate a common lower crust beneath this region. This gravity high is limited by a strong gravity gradient located in the deep crust ~70–150 km to the north of the geologically constrained boundary between the MAAW and EJTA units formed by the Erqis Zone (Fig. 13A). Importantly, the gravity map does not display any gravity anomaly over the two supposed and alternative traces of the Erqis Fault zone proposed by previous geological studies (e.g. Briggs et al., 2007; Xiao et al., 2009). Therefore, the gravity analysis shows that the Erqis Fault zone defined using questionable geological criteria does not display a prominent, deep-seated vertical discontinuity across all crustal levels typical for suture zones (Guy et al., 2020). Instead the EJTA dense crust continues far beneath southern part of the MAAW. This principal conclusion is tested using the forward magnetic and gravity modelling that was performed along a NE–SW striking cross-section perpendicular to the trend of the MAAW and the EJTA boundary (Jiang et al., 2016). The constraints applied to the modelled profile are: (1) the geological and geophysical interpretations provided by previous studies (Broussolle et al., 2018; Guy et al., 2020; Jiang et al., 2016) including the c. 30° dipping dense EJTA crust beneath the MAAW and the occurrences of ophiolite zones in the EJTA; (2) the Moho topography established by seismic and gravity studies (Guy et al., 2017; Wang et al., 2003;

Zhao et al., 2003); and (3) the density values assigned according to dominant lithologies forming both units, some of them deduced from thermodynamic modelling of metamorphic rocks (Jiang et al., 2016), and the magnetic susceptibility values from general tables (e.g. Clark and Emerson, 1991). Likewise for the southern Mongolia cross-section (Fig. 12D), the model of three layered crust with densities increasing with depth was set as the standard and maintained as much as possible through the iteration process using the GM-SYS program. The layered crust model was mainly kept beneath the Junggar Basin (Fig. 13C and D), where the densities and susceptibilities assigned to the EJTA are typical of an oceanic crust and an island arc system (Luo et al., 2017). The high density deep crustal layers and moderate magnetic susceptibilities reflect dominantly mafic to ultramafic composition of the Ordovician Zhaheba ophiolites associated with exhumed garnet amphibolite (Niu et al., 2009) or Silurian amphibolites exhumed in the central part of Yemaquan magmatic arc (Figs. 2, 11C and 13A; Luo et al., 2017). As in Mongolia, the intermediate density of the lower crust was deduced from isotopic mapping and chemistry of post-tectonic late Carboniferous-early Permian granitoids (Wang et al., 2017) and an important zircon inheritance of these granitoids (Zhang et al., 2017). The crustal structure of the MAAW is characterized by an intermediate density granulite-migmatite crust with a density of 2780 kg/m^3 which was exhumed in the magnetite-migmatite dome in the central part of the MAAW (Jiang et al., 2016). These high-grade rocks of mid-Devonian age also appear beneath the relatively less-dense amphibolite to greenschist facies rocks of the MAAW in the NE and probably also underneath the EJTA oceanic crust in the SW (Fig. 13B, C and D). At the boundary between the EJTA and the MAAW, a high amplitude magnetic signal is modelled by a steeply NE-dipping body, which corresponds to the Permian granulites containing magnetite (Fig. 10A).

5.4. Isotopic characterization of the lower crust in southern Mongolia and northwestern China

In the Mongolian sector, the nature of the lower crust was assessed also by means of geochemistry of Carboniferous and Permian granitoids intruding the EJTA oceanic crust (Figs.

2, 8 and 9; Guy et al., 2015). There, previous studies showed that a lower crustal continuity exists between the northerly MAAW and the southerly EJTA and that these two domains were characterized by intermediate to felsic lower crust of Cambro–Ordovician age. The redistribution of such a homogeneous lower crustal material had to occur before the early Carboniferous based on the oldest emplacement ages of the granitoids and the volcanic rocks of the EJTA (Guy et al., 2015; Nguyen et al., 2018). As in Mongolia, the character and composition of deeper crustal levels beneath the northwestern Chinese MAAW and EJTA are reconstructed from inferred sources of late Carboniferous–early Permian granitoids.

Using previous whole-rock studies for the MAAW and the EJTA granitoids (Buriánek et al., 2016; Cai et al., 2012, 2015; Gan et al., 2010; Guy et al., 2015; Liu et al., 2013; Shen et al., 2011; Tong et al., 2014; Yang et al., 2011; Zhang et al., 2017), the discrimination diagram of Jung et al. (2009) points mostly to metabasic (amphibolites) and quartzo-feldspathic (metagreywackes or orthogneisses) magma source (Figure 14A). In addition, sources of magmas from the northwestern Chinese EJTA included metapelitic rocks. Zircon Hf isotopic compositions from these granitic rocks provide important information about the mean crustal residence and the character of the magma sources from the studied units. The zircons from the northwestern Chinese EJTA have highly positive $\varepsilon_{Hf(t)}$ values (+10 to +16.6) with young two-stage Hf crustal model ages (c. 565 Ma). Also zircons from the southern Mongolian EJTA show positive $\varepsilon_{Hf(t)}$ values (+9.8 to +14.9) but slightly older two-stage Hf crustal model ages of c. 630 Ma (Figure 14B). On the other hand, zircons from the MAAW have significantly wider range of $\varepsilon_{Hf(t)}$ values (+3.5 to +15.4) and slightly higher two-stage Hf crustal model ages of c. 790 Ma in northwestern China and c. 890 Ma in southern Mongolia (Figure 14B). Altogether, whole-rock geochemical signatures and zircon Hf isotopic compositions of granitic rocks from the studied units display relatively small differences in the character and the model ages of magma sources. Moreover, the dominantly metabasic composition and juvenile character of the northwestern Chinese EJTA

crust is also confirmed by the compositions and isotopic characters of xenoliths entrapped in Cenozoic lavas (Zhang et al., 2017). The implication is that the Devonian–Carboniferous oceanic rocks of the whole EJTA was underplated by juvenile late Proterozoic–early Paleozoic metaigneous rocks of intermediate to felsic composition in Mongolia and intermediate to mafic metaigneous and metapelitic rocks in China before the Carboniferous magmatism.

6. DISCUSSION

Potential field data interpretation and modelling combined with geology and geochemistry provide significant insights into the geodynamic evolution of the southern tract of the Mongolian collage. We first discuss the similarities and differences of the geophysical responses between the southern Mongolian and the northwestern Chinese sectors of the CAOB. We then develop a concept of Permian–Triassic high-strain deformation zones between the Mongolian Precambrian blocks and the Tarim-North China cratons as deduced from both geophysical and geological observations. Based on an integrated geophysical, geological and isotopic mapping approach, we propose a new geodynamic scenario for both the Devonian accretion and the Permian–Triassic collision, which governed the formation of the Mongolian collage. Finally, we demonstrate how this major zone of deformation was reactivated during the Cenozoic convergence.

6.1. Similarities, differences and significance of geophysical anomalies in southern Mongolia and northwestern China

Geological and geophysical investigations of southern Mongolia and northwestern China show several first-order similarities. First, there is no match between the previously determined terrane boundaries (Badarch et al., 2002; Windley et al., 2002) and the geophysical lineaments (Guy et al., 2014b, 2020). In contrast, there is a remarkable continuity between NW–SE magnetic highs cross-cutting the presumed terrane boundaries in the southern Mongolian EJTA and those affecting northwestern Chinese EJTA and the southern part of the northwestern Chinese MAAW (Fig. 15A). In addition, both the MAAW and EJTA in southern Mongolia and in

northwestern China are characterized by NW–SE-trending equidistant and sub-parallel magnetic and gravity lineaments (Figs. 9B and C; 11B and C; Guy et al., 2015; 2020). In southern Mongolia and northwestern China, the linear anomalies are present in the upper crust (Figs. 12A and 13A) indicating important upper crustal lateral heterogeneity. In contrast, the lower crust beneath both domains shows remarkable absence of lineaments of any direction which indicates its rather homogeneous geophysical structure (Figs. 12A and 13A).

On the other hand, there are also important differences in both long wavelength and short wavelength gravity anomalies. The long wavelength gravity high is characteristic for the EJTA and the southern part of the northwestern Chinese MAAW, which indicates the presence of a high density and thick upper-middle crust beneath this region. In contrast, such an anomaly is lacking beneath the EJTA and MAAW in southern Mongolia implying a thin locally high density upper crust and a thicker homogeneous lower crust of intermediate density (Fig. 15). Despite different densities of the lower and upper crust between northwestern China and southern Mongolia, the late Paleozoic granitoids piercing these units indicates remarkable similarity in both crustal sources and zircon Hf isotopic signatures (Fig. 14B). The whole region corresponds to an isotopically homogeneous Hercynian province with late Proterozoic to late Cambrian (750–500 Ma) Nd and Hf model ages, highly positive ε_{Nd} (Kovalenko et al., 2004; Wang et al., 2017; Yarmolyuk et al., 2008, 2012; Wang et al., 2009) and ε_{Hf} values (Guy et al. 2015; Kröner et al., 2014; Sun et al., 2008). Reconciling the isotopic geochemistry with the geophysics is not an easy task but the higher density of the northwestern Chinese EJTA crust compared to the southern Mongolian EJTA crust might indicate juvenile material with some contribution of gabbros, amphibolites or mafic granulites in the source for the former region, whereas in the latter the source of granitoids is dominated by intermediate granulites and orthogneisses. However, the main argument for felsic and intermediate lower crust composition is in the typical chemistry of high-K calc-alkaline granitoids forming the bulk of late Carboniferous-early Permian intrusions

in the studied area, which according to Roberts and Clemens (1993) and Clemens (2012) can be generated only by partial melting hydrous, arc-related (calc-alkaline or high-K calc-alkaline) intermediate (andesitic or tonalitic) sources (Guy et al., 2015; Nguyen et al., 2018). In addition, the metasedimentary nature of the source of some late Carboniferous-early Permian granitoids intruding the East Junggar upper crust is reflected by the presence of xenocrystic/inherited <540 Ma zircons (Zhang et al., 2017), which perfectly match to zircons preserved in the northwestern Chinese MAAW gneisses and meta-sediments (Broussolle et al., 2019). Therefore, in the gravity models (Figs. 12 and 13) the lower crust of both the southern Mongolian and northwestern Chinese MAAW and EJTA could be modeled as a material of intermediate (2780 to 2730 kg/m^3) density based on the results of thermodynamic modelling of intermediate to felsic metaigneous and metasedimentary protoliths (Guy et al., 2015; Jiang et al., 2016).

Medium to high frequency magnetic anomalies in southern Mongolia closely correlate with the late Carboniferous–early Permian Gobi Tienshan and the Main Mongolian Lineament magmatic-volcanic zones (Fig. 8A; Kovalenko et al., 2004; Yarmolyuk et al., 2008). These zones are characterized by alkaline magmatism, large amounts of rhyolites, basalts and associated sediments, and were interpreted as narrow E–W trending intracontinental rifts. Similar signatures show a prominent magnetic high dividing the northwestern Chinese MAAW into a zone of Permian–Triassic magnetism in the south from zone dominated by the Devonian granitoids in the north (Figs. 11A and B). The source of this magnetic high is related to early Permian high temperature-low pressure (HT-LP) granulites and migmatites extruded within a tabular and vertical zone of deformation (Broussolle et al., 2018; 2019). Altogether, the Permian volcanic zones in southern Mongolia and HT-LP metamorphism in northwestern China contain magnetite in both magmatic and metamorphic rocks, which is a typical feature of this late Paleozoic event (Guy et al., 2015, 2020). In southern Mongolia, high frequency magnetic anomalies (Fig. 9B) correlate with NW–SE trending Permian–Triassic deformation zones due to

the preferential occurrence of highly magnetic serpentinites and gabbros in these zones (Guy et al., 2014a).

In general, high frequency gravity anomalies can be divided in two groups: (1) the NE–SW gravity lineaments, which are mainly developed in northwestern China, typically coincide with the Devonian orogenic fabric (Fig. 11A). These lineaments correspond to the alternations of NE–SW trending antiforms cored by the Devonian migmatites and granitoids, and synforms formed by the Ordovician and Devonian metasediments and metavolcanics (Guy et al., 2020); (2) almost orthogonal NW–SE trending gravity lineaments, which are observable in northwestern China and E-W trending high-frequency gravity anomalies in southern Mongolia . In southern Mongolia, these lineaments correspond to Permian–Triassic deformation zones affecting mainly the EJTA along which crop out high density rocks. In northwestern China the NW–SE trending anomalies coincide with deformation zones of similar age affecting both the EJTA and the southern part of the MAAW (Guy et al., 2020). Periodically spaced high frequency gravity anomalies document that the domain in between the Mongolian Precambrian blocks and the Tarim and North China cratons is structured by almost equidistant and sub-parallel array of deformation zones.

In the southern Mongolian EJTA, the high strain zones coincide with Permian-Triassic synforms that contain lenses of early Paleozoic ultramafic rocks (Guy et al., 2014a, Fig. 12C upper left inset). These periodically spaced synforms can be interpreted as upper crustal pop-down structures that are for instance described in Paleoproterozoic to Neoproterozoic accretionary orogens (Cagnard et al., 2007; Chardon et al., 2009). The analogue models of Cagnard et al. (2007) and Krýza et al., (submitted) show that such pop-down structures can typically develop when the layered crust, composed of rheologically weak intermediate to felsic lower crust and strong, dense and mafic upper crust, is affected by pure shear shortening (e.g. Chardon, 2009, Fig. 12C upper right inset). In southern Mongolia, the axial planes of synformal

structures are inclined to the north suggesting a global underthrusting of the South Gobi Zone beneath the EJTA and underthrusting of the EJTA upper crust beneath the MAAW during Permian –Triassic. The generalized N–S shortening of the rheologically weak EJTA and MAAW lower crust in front of the South Gobi rigid buttress results in the formation of high strain deformation zones associated with synformal pop downs of dense and strong upper crust similar to juvenile Proterozoic orogens (Chardon et al., 2009; Cagnard et al., 2011)

6.2. Contribution of geophysics to understand the geodynamic evolution of the Mongolian collage

Three main aspects in which the geophysical investigations provide an important contribution to the understanding of the geodynamic evolution of the southern branch of the Mongolian collage is discussed in this section : (1) Presence of the geophysically and isotopically homogeneous lower crust underneath Paleozoic sequences in southern Mongolia and northwestern China that can be interpreted in terms of a trench-directed lower crustal redistribution of the Lake Zone and MAAW crustal material related to the Devonian accretion processes. (2) Widespread occurrence of the equidistant and sub-parallel gravity and magnetic highs which correspond to deformation zones formed during the Permian–Triassic oroclinal bending. (3) Coincidence of these zones with a complex network of Cenozoic faults that originated during the intracontinental deformation resulting from the reactivation of the Permian–Triassic orogen at various scales.

6.2.1. Trench-directed lower crustal emplacement

One of the main contributions of combining the geophysical and isotopic geochemistry work of Guy et al. (2015) was the identification of a low density, intermediate-acid and homogeneous lower crust beneath the EJTA and the MAAW in southern Mongolia (Figs. 8 and 12). In addition, the predicted felsic to intermediate composition of the lower crust was confirmed by thermodynamic modelling based on the typical mineralogical compositions of lower crustal xenoliths trapped by Tertiary volcanics (Guy et al., 2015 and references therein).

The presence of such a homogeneous lower crust is also supported by magneto-telluric surveys showing a low resistivity and homogeneous layer in the depth range of 20 to 40 km (Comeau et al., 2018, 2020; Kaüfl et al., 2020). The geophysical, geological, geochemical and petrological data pointed towards a granulitized felsic to intermediate Cambrian arc-derived igneous and meta-sedimentary material, clearly allochthonous with respect to the overlying Silurian to Devonian oceanic crust. The rocks that best fit to this lower crustal allochthon are gabbros, diorites and tonalites of a giant ca. 1800 km long Cambro–Ordovician Ikh-Mongol Arc intruding Late Proterozoic accretionary wedges and ophiolites of the Lake Zone (Figs. 1 and 2; Janoušek et al., 2018). Another candidate is the product of early Devonian melting of Cambrian to Ordovician greywackes represented by intermediate granulites, migmatites and high grade gneisses frequently exposed in cores of migmatite domes in the MAAW (Jiang et al., 2015; Soejono et al., 2018). Jiang et al. (2016) shown that modeled density of high grade granulites derived from metasedimentary arc related rocks correspond to those originating from HT metamorphism of igneous protoliths. The timing of the flow of these highly mobile rocks beneath the EJTA and the MAAW crust is not precisely constrained. However, based on the early Carboniferous ages (350–330 Ma) of the oldest magmatic rocks piercing the EJTA, it is thought to have occurred in the late Devonian. This is also an age of the main folding event affecting this domain (Guy et al., 2014a; Lehmann et al. 2010), which is characterized by the exhumation of a hot partially molten material in the MAAW (e.g. Jiang et al., 2015; Broussolle et al., 2015). It is supposed that during this event low viscosity juvenile crust was laterally redistributed beneath the supra-subduction oceanic crust in the trench direction from the shortened MAAW (Guy et al., 2015; Nguyen et al., 2018). As a result, the 10–12 km thick oceanic, intraoceanic arc or back-arc basin crust of the EJTA (Lamb and Badarch, 2001) was underplated by an allochthonous felsic material from the rear part of the orogenic system. The global geometry of the system is illustrated by Figure 16C showing the emplacement of the Ikh Mongol Arc and the MAAW derived partially molten rocks

beneath the EJTA at the pro-wedge side, and the concomitant subduction of the oceanic crust (Paleo-Asian Ocean in Fig. 16A) at the retro-wedge side of the system.

Such a lower crustal emplacement probably operated in northwestern China as well, as indicated by the similar isotopic signature of late Carboniferous–early Permian granitoids piercing the EJTA Paleozoic basement or intruding the MAAW and <540 Ma ages of xenocrystic zircons preserved in some intrusions (Zhang et al., 2017). The only difference is the high density of the EJTA Paleozoic middle crust which also supports the exposed mafic and ultramafic metamorphic rocks (Luo et al., 2017; Niu et al., 2009). We propose that as in southern Mongolia, juvenile, highly mobile crust was emplaced beneath the EJTA mafic crust during late Devonian compression (Jiang et al., 2015; Zhang et al., 2015). The resulting geometry of the system was defined by the trench-directed lower crustal flow with higher contribution of the MAAW metasedimentary rocks compared to dominant metaigneous rocks of the Mongolian counterpart (Fig.16C).

6.2.2. Permian–Triassic oroclinal bending and development of vertical deformation zones

At the scale of the whole southern part of Mongolian collage, magnetic and isostatic residual gravity anomalies reveal a periodicity of the signal correlating with vertical zones of intense deformation (Guy et al., 2014b, 2020). The width of these magnetic and gravity highs varies from 10 to 30 km and the length can reach up to few hundreds of kilometers (Figs. 8, 9 and 13). The 2D forward magnetic and gravity modelling in southern Mongolia indicated that these high-strain zones can be deeply rooted, up to ~20 km depth (Guy et al., 2015). The surface locations of the high-strain zones can be detected by the magnetic and gravity signals since there are significant contrasts in the magnetic susceptibilities and the densities between these vertical zones and the sub-horizontal low strain domains. This is because in the cores of the high-strain zones are exhumed high-grade metamorphic, mafic volcanic and ultramafic rocks (Guy et al., 2014b) characterized by high magnetic susceptibility and density values. In summary, all late

Proterozoic to early Paleozoic sequences in southern Mongolia were heterogeneously deformed by an array of steeply dipping E–W trending deformation zones of Permian–Triassic age. Lehmann et al. (2010) and Edel et al. (2014) showed that these zones are intimately related to the mechanism of an oroclinal bending, in particular with the anticlockwise rotation of the southern flank of the Mongolian orocline (Fig. 16A). Here, the Permian–Triassic deformation zones can be seen as a crustal scale crenulation cleavage, which reworked previous Devonian fabrics and tectonic boundaries in a regular manner. These deformation features are well illustrated by high frequency magnetic and gravity anomalies in both studied regions (Fig. 16C).

In northwestern China, the effects of the Permian–Triassic deformation are different because of the mafic composition and consequent higher strength of the EJTA middle and upper imbricated crusts. This dense basement block played the role of a strong indentor which was underthrust beneath the northwestern Chinese MAAW generating a wide zone of Permian deformation in the southern part of the latter unit. The previous study of Guy et al. (2020) indicated that the underthrusting of the EJTA promontory beneath the Chinese MAAW was responsible for the extrusion of partially molten rocks of Permian age along a tabular deformation zone (Fig. 16C) defined by Broussolle et al. (2018). This granulite facies zone is parallel to NW–SE trending greenschist facies thrusts and transpressive zones of Permian–Triassic age affecting both the southern part of the northwestern Chinese MAAW and the EJTA (Briggs et al:, 2007; Li et al., 2016). All these structural features are well defined by linear magnetic highs (Figs. 11A and B; 16C).

An important implication is that during Permian to Triassic, the Paleozoic sequences of the whole southern flank of the Mongolian orocline were reworked, changing orientation from E–W in the limb (southern Mongolia) to NW–SE (northwestern China) towards the hinge of the Mongolian orocline. This deformation zone is the most spectacular feature of the Mongolian collage as it reflects extreme shortening up to several hundred percent of all Paleozoic sequences

between the rigid Mongolian Precambrian blocks in the north and the Tarim-North-China cratons in the south (Edel et al., 2014).

6.2.3. Geophysical features related to the Cenozoic deformation of the Mongolian collage

Since the Cenozoic, the CAOB has been evolving as an intracontinental orogen leading to transpressive faulting and thrusting, which accommodate the India-Eurasia collision (Molnar and Tapponier, 1975; Calais et al., 2003; Cunningham et al., 2003; 2009). Cunningham et al. (2003) identified NW–SE dextral Cenozoic faults affecting the Paleozoic sequences of northwestern China, while in southern Mongolia Cunningham et al. (2005) described sinistral E–W trending Cenozoic faults. Associated topographic features corresponding to NW–SE and E–W trending mountain ranges in the respective domains were interpreted as restraining bends. This general pattern was summarized by Cunningham (2013) who proposed that during the Cenozoic, the Paleozoic units in the west were affected by major dextral transpression, whereas the corresponding units in the east suffered a sinistral transpressional deformation. This difference in orientation of restraining bends and kinematics of transpressional faults was attributed to northward movements of the Tarim indentor and the shape of the passive Mongolian Precambrian block (Cunningham, 2013; Cunningham et al., 2003).

Guy et al. (2014b) compared the residual gravity map with the southern Mongolia topographic map and concluded that a large number of the prominent NW–SE trending mountain ranges in the EJTA corresponds to gravity highs. These authors interpreted the linear gravity anomalies as the geophysical expressions of Permian–Triassic deformation zones reactivated during the Cenozoic convergence. In this present review, we further extended the comparison of gravity and magnetic lineaments with the Cenozoic fault networks identified by Cunningham et al. (2003; 2009) and Cunningham (2005; 2007; 2013) in the whole southern part of the Mongolian collage (Fig. 17). This comparison shows a good match of the geophysical lineaments and the NW–SE dextral Cenozoic faults in northwestern China and western

Mongolia (orange direction in rose diagrams, inset in Fig. 17A) with the exception of few N–S trending dextral faults (highlighted blue directions in rose diagrams, inset in Fig. 17A). On the other hand most of the NNE–SSW trending gravity anomalies corresponding to the Devonian structures do not correlate with the Cenozoic faults (green lines in Fig. 17B). There is also a good correlation between gravity lineaments and NW–SE-oriented restraining bends in southern Mongolia (highlighted orange directions in rose diagrams, inset in Fig. 17A) with exception of the most important Gobi-Tienshan or Bogd sinistral strike-slip faults (highlighted blue E–W direction in rose diagrams, inset in Fig. 17A). In this region, neither geophysical anomalies nor the Cenozoic faults match with the Devonian fabrics that are oriented generally NW–SE (e.g. Edel et al., 2014; Lehmann et al., 2010) with exception of splays at both western and eastern terminations of the prominent Gobi-Tienshan Fault.

The strong correlation between both dextral and sinistral faults and geophysical anomalies that originated during the Permian–Triassic deformation suggests an important role of the Cenozoic reactivation of the inherited structures. We suggest that these Permian–Triassic steep zones were exploited in response to the NE directed Cenozoic stress field compatible with the activity of large Cenozoic sinistral lithospheric faults accommodating the lateral escape of central Asia caused by northward movement of India (Zhang et al., 2004). Altogether, the variable orientation of the Permian–Triassic deformation zones around the Mongolian Precambrian blocks played a pivotal role in the accommodation of the Cenozoic continental intraplate deformation north of the Tarim-North China cratons (Cunningham et al., 2003; Cunningham, 2013).

The periodic alternation of E–W and NW–SE trending mountain ranges with the Cenozoic depressions in Mongolia shows a crustal wavelength of 30–50 km (Figs. 1A and 2), which was interpreted as a result of crustal folding (Burov et al., 1993; Nikishin et al., 1993). Thus, the first-order morphological features like the Altai and Tien Shan mountain ranges were

interpreted as a result of flexural folding of the lithosphere. However, our study shows that first-order topographic features are mainly related to the Cenozoic reactivation of Permian–Triassic upper crustal steep deformation zones. Similarly, the Altai and Tien Shan mountain ranges, associated with significant increases of the Moho depth (Guy et al., 2017), correlate well with the positions of the crustal scale Paleozoic tectonic units e.g. Tien Shan subduction wedge in the south and the MAAW in the north (Xiao et al., 2015). It is therefore likely, that the spacing and periodicity of central Asian topographic features at least partly result from Cenozoic reactivation of principal Paleozoic–Mesozoic structural elements of various scales.

7. CONCLUSIONS

- Magnetic and gravity data suggest the inconsistencies between geologically defined terranes and geophysical domains in the scale of the Mongolian collage.
- Magnetic and gravity analysis and modelling combined with whole-rock geochemistry of Carboniferous–Permian granitoids show the presence of a lower crustal felsic to intermediate juvenile material beneath the geophysically heterogeneous upper crust. This feature is interpreted as a result of a trench-directed lower crustal emplacement of an arc beneath the Paleozoic oceanic crust.
- The potential field data confirmed the presence of N–S to NE–SW late Devonian and E–W to NW–SE Permian–Triassic deformation fabrics.
- The gravity and magnetic anomalies highlight a periodicity of the signal correlating with the alternation of Permian–Triassic high and low strain zones in the Altai deformation domain wrapping around the hinge of the Mongolian orocline. This Altai deformation domain results from the post-oroclinal shortening of the Paleozoic units between the Mongolian Precambrian blocks in the north and the Tarim-North China cratons in the south.

- During the Cenozoic convergence, both Paleozoic and Mesozoic structural elements played major roles in the kinematics and orientation of the Tertiary faults in the southern part of the Mongolian collage.

ACKNOWLEDGMENTS

This study was funding by the Grant Agency of the Czech Republic (GAČR EXPRO grant GX19-27682X). The EGM08 at 2.5×2.5 arc minute was downloaded at: http://bgi.obs-mip.fr/data-products/Grids-and-models/regional_gravity_anomaly_grids). This review would not be possible without fruitful and constructive discussions with Vojtech Janoušek, Robin Armstrong, Reimar Seltmann and Alla Dolgopolova. This is a contribution to IGCP 662.

The authors thank the constructive and stimulating comments of David Moore and an anonymous reviewer. We also thank Nicholas Rawlinson for his editorial work.

FIGURE CAPTIONS

Figure 1: A. Topography map of Central Asia from ETOPO1 (modified from Amante and Eakins, 2009) with the two studied area of this review outlined by the black boxes. B. Global tectonic map of the CAOB (modified from Parfenov et al., 2003) with the location of the two forward modelling profiles.

Figure 2: Detailed geological maps of northwestern China (modified from Broussolle et al., 2018; Guy et al., 2020) and southern Mongolia (modified from Guy et al., 2014b) with the superimposed tectonic zones (thick black lines). In transparency is the Tectonic map of the Mongolian collage system constituting the central part of the CAOB (modified from Parfenov et al., 2003; Jiang et al., 2017).

Figure 3: Simplified lithostratigraphic columns of the Paleozoic and Mesozoic rocks for the five tectonic zones described in this study (modified from Guy et al., 2015).

Figure 4: Spatial coverage and methods of the previous potential field analysis.

Figure 5: Mongolian collage potential field data. (A) Magnetic map extracted from EMAG2 (Maus et al., 2009) and reduced to the pole and (B) isostatic residual gravity anomaly map derived from EGM08 (Pavlis et al., 2012). The dashed squares located the study areas of this paper in southern Mongolia and northwestern China. All the anomaly maps in this and the followings similar figures are displayed using a linear scale.

Figure 6: Southern Mongolia potential field maps. A. Airborne magnetic map reduced to the pole superimposed on the EMAG2. B. Isostatic residual gravity anomaly map from the

DSCN08. The black rectangles indicate the locations of the comparison between the geophysical signal responses and the geology.

Figure 7: Northwestern China potential field maps. A. Magnetic map from EMAG2. B. Isostatic residual gravity anomaly map from EGM08 model. The black rectangles indicate the location of the comparison between the geophysical signal and the geology.

Figure 8: Comparison between potential field signals and geology in southern Mongolia. A. Regional magnetic highs correspond to magmatic provinces, which were defined by Kovalenko et al. (2006); GTRZ: Gobi-Tienshan Rift Zone; MMLRZ: Main Mongolian Lineament Rift Zone. B. Regional gravity lineaments are correlated with high-strain zones (modified from Guy et al., 2014b). The legend of the geological map in B is the same than the legend in figure 2. Locations of Figures 8A and 8B shown on Figure 6.

Figure 9: Correlation between potential field fabrics and the deformation phases (modified from Guy et al, 2014b; Lehmann et al., 2010). A. Geological map of southern Mongolia. The legend of the geological map is the same than the legend in figure 2. The boxes indicate the locations of detailed geological studies. B. Juxtaposition of the tilt and matched-filtering resulting magnetic lineaments superimposed on the magnetic anomaly map reduced to the pole and the resulting rose diagram of the three groups. The white zones are the magnetic highs corresponding to magmatic provinces. C. Gravity lineaments superimposed on the isostatic residual gravity anomaly map. The white zones are the gravity highs corresponding to the Permian–Triassic high-strain zones. Rose diagrams discriminate the tendency of three groups common to magnetic and gravity anomalies (PolyLX, https://petrol.natur.cuni.cz/~ondro/oldweb/polylx:home). D. Table of the stereonets relating the deformation phases to the tectonic zones representing poles of foliations in equal area lower hemisphere projections.

Figure 10: Comparison between potential field signals and geology in northwestern China. A. The main magnetic high corresponds to the Permian magnetite-bearing granulites. B. NE–SW and NW–SE gravity lineaments respectively correspond to the Devonian (S_2) and Permian (S_3) structural fabrics (modified from Guy et al., 2020). The inset displays the tilt derivative map in order to exemplify the continuation to the NE of the NE-SW lineament. Locations of Figures 10A and 10B shown on Figure 7.

Figure 11: Correlation between potential field fabrics and the deformation phases (modified from Guy et al., 2020). A. Geological map of northwestern China. The legend of the geological map is the same than the legend in figure 2. The boxes indicate the locations of detailed geological studies. B. Juxtaposition of the tilt and matched-filtering resulting magnetic lineaments superimposed on the magnetic anomaly map reduced to the pole and the resulting rose diagram of the three groups. The white zones represented the high-strain zones. C. Gravity lineaments superimposed on the isostatic residual gravity anomaly map and the resulting rose diagram of the three groups (PolyLX, https://petrol.natur.cuni.cz/~ondro/oldweb/polylx:home). The white zones represented the magmatic provinces. The rose diagrams B and C include data from the entire map. D. Table of the stereonets relating the deformation phases to the tectonic zones representing poles of foliations in equal area lower hemisphere projection.

Figure 12: 2D forward model along profile A-A' in southern Mongolia. A. Magnetic and isostatic residual gravity and long-wavelength complete Bouguer depth sliced (source layer at 39 km) anomaly maps to visualize the trends of the upper and deep crustal signals. The thick black curves underline the global trend of magnetic and gravity highs. The white lines represent the tectonic boundaries. The grey line is the state border. Location shown on Figure 1. B. Observed and calculated magnetic and gravity data. C. Simplified geological cross-section along the profile A-A'. D. Global structure of the crust in southern Mongolia from magnetic and gravity forward modelling profile. Unit of density = kg/m^3; unit of susceptibility=SI. vol.-sed.: volcano-sediments.

Figure 13: 2D forward model along profile B-B' in northwestern China. A. Magnetic and isostatic residual gravity and long-wavelength complete Bouguer depth sliced (source layer at 44 km) anomaly maps to visualize the trends of the upper and deep crustal signals. The thick black curves underline the global trend of magnetic and gravity highs. The dashed blue curves represent the geologically defined Erqis traces. The small black areas locate the ophiolites. The grey lines are the state borders. B. Observed and calculated magnetic and gravity data. C. Simplified geological cross-section along the profile B-B'. D. Global structure of the crust in northwestern China from magnetic and gravity forward modelling profile. Unit of density = kg/m^3; unit of susceptibility=SI. vol.-sed.: volcano-sediments.

Figure 14: A. Discrimination diagrams of crustal sources of granitic magmas and zircon Hf isotopic composition of the late Carboniferous–early Permian crust-derived granitoids from the East Junggar Trans-Altai and Mongol Altai Accretionary Wedge. Binary plot $Al_2O_3 + FeOt + MgO + TiO_2$ vs. $Al_2O_3/(FeOt + MgO + TiO_2)$ of Jung et al. (2009). B. Recalculated published zircon Hf isotopic data. $\varepsilon_{Hf(t)}$ vs. age diagram and two-stage Hf model ages. ^{176}Lu decay constant of Scherer et al. (2001), CHUR values of Blichert-Toft and Albarède (1997) and DM values of Griffin et al. (2004) were used.

Figure 15: Comparison of main geophysical fabrics vs. structure of the upper and the lower crust. A. Magnetic fabrics superimposed on tectonic zones and upward continuation of magnetic data to 50 km. B. Gravity fabrics superimposed on tectonic zones and upward continuation of Bouguer data to 20 km.

Figure 16: A. Schematic model for the Late Paleozoic geodynamic evolution of the Mongolian collage B. with detailed subareas of northwestern China and southern Mongolia. C. Idealized cross-sections through the corresponding tectonic zones with their main geochemical and geophysical characteristics. LZ: Lake Zone; MAAW: Mongol Altai Accretionary Wedge; SGZ: South Gobi Zone; EJTA: East Junggar Trans-Altai; TM: Tuva-Mongol. Bf.: Bogd Fault; Bul.f.: Bulgan Fault; GTf.: Gobi-Tienshan Fault.

Figure 17: Permian–Triassic high-strain zones form a corridor highlighted by the two thick yellow curves. A. Vertical derivative of the isostatic residual gravity anomaly map and B. Vertical derivative of the magnetic anomaly map with the network of the Cenozoic faults described by Cunningham (2013) in black and the gravity and magnetic lineaments in white and grey respectively. The color of the rose diagrams correspond to the colors of the faults and geophysical lineaments in the maps.

REFERENCES

Aitken, A.R.A., Betts, P.G., Weinberg, R.F., Gray, D., 2009. Constrained potential field modeling of the crustal architecture of the Musgrave Province in central Australia: Evidence for lithospheric strengthening due to crust- mantle boundary uplift. Journal of Geophysical Research 114.

Al-Chalabi, M., 1971. Some Studies Relating to Nonuniqueness in Gravity and Magnetic Inverse Problems. Geophysics 36, 5.

Amante, C., Eakins, B.W., 2009. ETOPO1 1 Arc-Minute Global Relief Model: Procedures, Data Sources and Analysis. NOAA Technical Memorandum NESDIS NGDC, 19-24.

An, S., Zhou, K., Wang, J., Yang, H., Zhang, Z., 2018. Integrated analysis of gravity and magnetic fields in the Eastern Tianshan Belt, Xinjiang, Central Asia: Implications for Cu-Au-Fe polymetallic deposits exploration. Journal of Applied Geophysics 159, 319-328.

Andersen, O.B., Knudsen, P., 2009. DNSC08 mean sea surface and mean dynamic topography models. Journal of Geophysical Research-Oceans 114.

Badarch, G., Cunningham, D.W., Windley, B.F., 2002. A new terrane subdivision for Mongolia: implications for the Phanerozoic crustal growth of Central Asia. Journal of Asian Earth Sciences 21, 87-110.

Banka, D., Pharaoh, T.C., Williamson, J.P., 2002. Potential field imaging of Palaeozoic orogenic structure in northern and central Europe. Tectonophysics 360, 23-45.

Barry, T.L., Saunders, A.D., Kempton, P.D., Windley, B.F., Pringle, M.S., Dorjnamjaa, D., Saandar, S., 2003. Petrogenesis of Cenozoic Basalts from Mongolia: Evidence for the Role of Asthenospheric versus Metasomatized Lithospheric Mantle Sources. Journal of Petrology 44, 55-91.

BGMR, Xinjiang, 1966. Geologic map of the M - 45 - XXXIV area: Unpublished, scale 1:200,000, 1 sheet.

Blichert-Toft, J., Albarède, F., 1997. The Lu-Hf isotope geochemistry of chondrites and the evolution of the mantle-crust system. Earth and Planetary Science Letters 148, 243-258.

Bold, U., Crowley, J.L., Smith, E.F., Sambuu, O., Macdonald, F.A., 2016. Neoproterozoic to early Paleozoic tectonic evolution of the Zavkhan terrane of Mongolia: Implications for continental growth in the Central Asian orogenic belt. Lithosphere 8, 729-750.

Braitenberg, C., Ebbing, J., 2009. New insights into the basement structure of the West Siberian Basin from forward and inverse modeling of GRACE satellite gravity data. Journal of Geophysical Research: Solid Earth 114.

Briggs, S.M., Yin, A., Manning, C.E., Chen, Z.L., Wang, X.F., Grove, M., 2007. Late Paleozoic tectonic history of the Ertix Fault in the Chinese Altai and its implications for the development of the Central Asian Orogenic System. Bulletin of the Geological Society of America 119, 944.

Broussolle, A., Aguilar, C., Sun, M., Schulmann, K., Štípská, P., Jiang, Y., Yu, Y., Xiao, W., Wang, S., Míková, J., 2018. Polycyclic Palaeozoic evolution of accretionary orogenic wedge in the southern Chinese Altai: Evidence from structural relationships and U–Pb geochronology. Lithos 314-315, 400-424.

Broussolle, A., Sun, M., Schulmann, K., Guy, A., Aguilar, C., Štípská, P., Jiang, Y., Yu, Y., Xiao, W., 2019. Are the Chinese Altai "terranes" the result of juxtaposition of different crustal levels during Late Devonian and Permian orogenesis? Gondwana Research 66, 183-206.

Broussolle, A., Štípská, P., Lehmann, J., Schulmann, K., Hacker, B.R., Holder, R., Kylander-Clark, A.R.C., Hanžl, P., Racek, M., Hasalová, P., Lexa, O., Hrdličková, K., Buriánek, D., 2015. P−T−t−D record of crustal-scale horizontal flow and magma assisted doming in the SW Mongolian Altai. Journal of Metamorphic Geology, 24.

Buriánek, D., Janousek, V., Hanzl, P., Jiang, Y., Schulmann, K., Lexa, O., Altanbaatar, B., 2016. Petrogenesis of the Late Carboniferous Sagsai Pluton in the SE Mongolian Altai. Journal of Geosciences 61, 67-92.

Buriánek, D., Schulmann, K., Hrdličková, K., Hanžl, P., Janoušek, V., Gerdes, A., Lexa, O., 2017. Geochemical and geochronological constraints on distinct Early-Neoproterozoic and Cambrian accretionary events along southern margin of the Baydrag Continent in western Mongolia. Gondwana Research 47, 200-227.

Burov, E.B., Houdry, F., Diament, M., Déverchère, J., 1994. A broken plate beneath the North Baikal Rift Zone revealed by gravity modelling. Geophysical Research Letters 21, 129-132.

Burov, E.B., Lobkovsky, L.I., Cloetingh, S., Nikishin, A.M., 1993. Continental lithosphere folding in Central Asia (part II): Constraints from gravity and topography. Tectonophysics 226, 73-87.

Buslov, M. M., I. Y. Safonova, T. Watanabe, O. T. Obut, Y. Fujiwara, K. Iwata, N. N. Semakov, Y. Sugai, L. V. Smirnova, and A. Y. Kazansky, 2001. Evolution of the Paleo-Asian Ocean (Altai-Sayan Region, Central Asia) and collision of possible Gondwana-derived terranes with the southern marginal part of the Siberian continent, Geosciences Journal, 5(3), 203.

Cai, K., Sun, M., Jahn, B.-m., Xiao, W., Yuan, C., Long, X., Chen, H., Tumurkhuu, D., 2015. A synthesis of zircon U–Pb ages and Hf isotopic compositions of granitoids from Southwest Mongolia: Implications for crustal nature and tectonic evolution of the Altai Superterrane. Lithos 232, 131-142.

Cai, K., Sun, M., Yuan, C., Xiao, W., Zhao, G., Long, X., Wu, F., 2012. Carboniferous mantle-derived felsic intrusion in the Chinese Altai, NW China: Implications for geodynamic change of the accretionary orogenic belt. Gondwana Research 22, 681-69[illegible]

Cagnard, F., Barbey, P., Gapais, D., 2011. Transition between "Archaean-type" and "modern-type" tectonics: Insights from the Finnish Lapland Granulite Belt. Precambrian Research, 187, 127-142.

Cagnard, F., Durrieu, N., Gapais D., Brun, J.P., Ehlers, C., 2007. Crustal thickening and lateral flow during compression of hot lithospheres, with particular reference to Precambrian times. Terra Nova, 18 (1), 72-78.

Calais, E., Vergnolle, M., Sankov, V., Lukhnev, A., Miroshnitchenko, A., Amarjargal, S., Deverchere, J., 2003. GPS measurements of crustal deformation in the Baikal-Mongolia area (1994-2002): Implications for current kinematics of Asia. J. Geophys. Res. 108.

Cawood, P.A., Kröner, A., Collins, W.J., Kusky, T.M., Mooney, W.D., Windley, B.F., 2009. Accretionary orogens through Earth history. Geological Society, London, Special Publications 318, 1.

Chardon, D., Gapais, D., Cagnard, F., 2009. Flow of ultra-hot orogens: A view from the Precambrian, clues for the Phanerozoic. Tectonophysics, 477, 105-118.

Charles, N., Gumiaux, C., Augier, R., Chen, Y., Faure, M., Lin, W., Zhu, R., 2012. Metamorphic Core Complex dynamics and structural development: Field evidences from the Liaodong Peninsula (China, East Asia). Tectonophysics 560–561, 22-50.

Christensen, N.I., Mooney, W.D., 1995. Seismic velocity structure and composition of the continental crust: a global view. Journal of Geophysical Research 100, 9761-9788.

Clark, D. A., and J. B. Emerson, 1991. Notes On Rock Magnetization Characteristics In Applied Geophysical Studies, Explor. Geophys., 22(3), 547-555.

Clemens, J.D., 2012. Granitic magmatism, from source to emplacement: a personal view. Applied Earth Science 121, 107-136.

Cogné, J.P., Kravchinsky, V.A., Halim, N., Hankard, F., 2005. Late Jurassic-Early Cretaceous closure of the Mongol-Okhotsk Ocean demonstrated by new Mesozoic palaeomagnetic results from the Trans-BaiÌˆkal area (SE Siberia). Geophysical Journal International 163, 813.

Comeau, M.J., Becken, M., Käufl, J.S., Grayver, A.V., Kuvshinov, A.V., Tserendug, S., Batmagnai, E., Demberel, S., 2020. Evidence for terrane boundaries and suture zones across Southern Mongolia detected with a 2-dimensional magnetotelluric transect. Earth, Planets and Space 72, 5.

Comeau, M. J., J. S. Käufl, M. Becken, A. Kuvshinov, A. V. Grayver, J. Kamm, S. Demberel, U. Sukhbaatar, and E. Batmagnai, 2018. Evidence for fluid and melt generation in response to an asthenospheric upwelling beneath the Hangai Dome, Mongolia, Earth and Planetary Science Letters, 487, 201-209.

Cunningham, D., 2005. Active intracontinental transpressional mountain building in the Mongolian Altai: Defining a new class of orogen. Earth and Planetary Science Letters 240, 436.

Cunningham, D., 2007. Structural and topographic characteristics of restraining bend mountain ranges of the Altai, Gobi Altai and easternmost Tien Shan. Geological Society, London, Special Publications 290, 219.

Cunningham, D., 2013. Mountain building processes in intracontinental oblique deformation belts: Lessons from the Gobi Corridor, Central Asia. Journal of Structural Geology 46, 255-282.

Cunningham, D., Davies, S., McLean, D., 2009. Exhumation of a Cretaceous rift complex within a Late Cenozoic restraining bend, southern Mongolia: Implications for the crustal evolution of the Gobi Altai region. Journal of the Geological Society 166, 321-333.

Cunningham, D., Dijkstra, A., Howard, J., Quarles, A., Badarch, G., 2003. Active intraplate strike-slip faulting and transpressional uplift in the Mongolian Altai. Geological Society, London, Special Publications 210, 65.

Cunningham, W. D., B. F. Windley, D. Dorjnamjaa, G. Badamgarov, and M. Saandar, 1996. A structural transect across the Mongolian Western Altai: Active transpressional mountain building in central Asia, Tectonics, 15(1), 142-156.

Daoudene, Y., Gapais, D., Ledru, P., Cocherie, A., Hocquet, S., Donskaya, T.V., 2009. The Ereendavaa Range (north-eastern Mongolia): An additional argument for Mesozoic extension throughout eastern Asia. International Journal of Earth Sciences 98, 1381-1393.

Daoudene, Y., Gapais, D., Ruffet, G., Gloaguen, E., Cocherie, A., Ledru, P., 2012. Syn-thinning pluton emplacement during Mesozoic extension in eastern Mongolia. Tectonics 31.

Darby, B.J., Davis, G.A., Zhang, X., Wu, F.Y., Wilde, S.A., Yang, J.H., 2004. The newly discovered Waziyu metamorphic core complex, YiwuliJ Shan, western Liaoning Province, Northwest China. Earth Science Front 11, 145-155.

Dhuime, B., Hawkesworth, C.J., Cawood, P.A., Storey, C.D., 2012. A change in the geodynamics of continental growth 3 billion years ago. Science 335, 1334-1336.

Dobretsov, N.L., Buslov, M.M., Rubanova, E.S., Vasilevsky, A.N., Kulikova, A.V., Bataleva, E.A., 2017. Middle-Late Paleozoic geodynamic complexes and structure of Gorny Altai and their record in gravity data. Russian Geology and Geophysics 58, 1277-1288.

Edel, J.B., Schulmann, K., Hanžl, P., Lexa, O., 2014. Palaeomagnetic and structural constraints on 90° anticlockwise rotation in SW Mongolia during the Permo–Triassic: Implications for Altaid oroclinal bending. Preliminary palaeomagnetic results. Journal of Asian Earth Sciences 94, 157-171.

Gan, L., Tang, H.F., Han, Y.J., 2010. Geochronology and geochemical characteristics of the Yemaquan granitic pluton in East Junggar, Xinjiang. Acta Petrologica Sinica 26, 2374-2389.

Glen, J.M.G., Schmidt, J., Morin, R., 2007. Gravity and magnetic character of south-central alaska: Constraints on geologic and tectonic interpretations, and implications for mineral exploration, in: Ridgway, K.D., Trop, J.M., Glen, J.M.G., O'Neill, J.M. (Eds.), Tectonic Growth of a Collisional Continental Margin: Crustal Evolution of Southern Alaska. Geological Society of America, Special Papers, pp. 593-622.

Griffin, W.L., Belousova, E.A., Shee, S.R., Pearson, N.J., O'Reilly, S.Y., 2004. Archean crustal evolution in the northern Yilgarn Craton: U–Pb and Hf-isotope evidence from detrital zircons. Precambrian Research 131, 231-282.

Guy, A., Holzrichter, N., Ebbing, J., 2017. Moho depth model for the Central Asian Orogenic Belt from satellite gravity gradients. Journal of Geophysical Research: Solid Earth 122, 7388-7407.

Guy, A., Schulmann, K., Clauer, N., Hasalová, P., Seltmann, R., Armstrong, R., Lexa, O., Benedicto, A., 2014a. Late Paleozoic–Mesozoic tectonic evolution of the Tarbagatai-Altai and South Gobi Zones in southern Mongolia based on structural and geochronological data. Gondwana Research 25, 309-337.

Guy, A., Schulmann, K., Janoušek, V., Štípská, P., Armstrong, R., Belousova, E., Dolgopolova, A., Seltmann, R., Lexa, O., Jiang, Y., Hanžl, P., 2015. Geophysical and geochemical nature of relaminated arc-derived lower crust underneath oceanic domain in southern Mongolia. Tectonics 34, 1030-1053.

Guy, A., Schulmann, K., Munschy, M., Miehe, J.-M., Edel, J.-B., Lexa, O., Fairhead, D., 2014b. Geophysical constraints for terrane boundaries in southern Mongolia. Journal of Geophysical Research: Solid Earth 119, 7966-7991.

Guy, A., Schulmann, K., Soejono, I., Xiao, W., 2020. Revision of the Chinese Altai - East Junggar terrane accretion model based on geophysical and geological constraints. Tectonics, e2019TC006026.

Hacker, B.R., Kelemen, P.B., Behn, M.D., 2011. Differentiation of the continental crust by relamination. Earth and Planetary Science Letters 307, 501-516.

Hanžl, P., Guy, A, Batsaikhan, A, Lexa, O., Schulmann, K., Kunceová, E., Hrdličková, K., Janoušek, V., Buriánek, D., Krejčí, Z., Jiang, Y., Otgonbaatar, D., 2020. Geology of the Gobi and Mongol Altai junction enhanced by gravity analysis: a key for understanding of the Mongolian Altaides, Journal of Maps, 16(2), 98-107.

Heiskanen, W.A., Moritz, H., 1967. Physical Geodesy. W. H. Freeman and Company, San Francisco.

Hinze, W.J., von Frese, R.R.B., Saad, A.H., 2013. Gravity and Magnetic Exploration: Principles, Practices, and Applications. Cambridge University Press, Cambridge.

Hirt, C., Rexer, M., 2015. Earth2014: 1 arc-min shape, topography, bedrock and ice-sheet models – Available as gridded data and degree-10,800 spherical harmonics. International Journal of Applied Earth Observation and Geoinformation 39, 103-112.

Jahn, B.M., 2004. The Central Asian Orogenic Belt and growth of the continental crust in the Phanerozoic, in: Malpas, J., Fletcher, A., Ali, J.R., Aitchison, J.C. (Eds.), Aspects of the Tectonic Evolution of China. Geological Society London Special Publications 226, pp. 73-100.

Janoušek, V., Jiang, Y., Buriánek, D., Schulmann, K., Hanžl, P., Soejono, I., Kröner, A., Altanbaatar, B., Erban, V., Lexa, O., Ganchuluun, T., Košler, J., 2018. Cambrian–Ordovician magmatism of the Ikh-Mongol Arc System exemplified by the Khantaishir Magmatic Complex (Lake Zone, south–central Mongolia). Gondwana Research 54, 122-149.

Jiang, Y.D., Schulmann, K., Sun, M., Štípská, P., Guy, A., Lexa, O., Janoušek, V., Yuan, C., 2017. Melting of accretionary wedge and building mature continental crust: Insights from the magmatic evolution of the Chinese altai orogen, central Asia. Geodynamics and Tectonophysics 8, 481-482.

Jiang, Y.D., Schulmann, K., Sun, M., Weinberg, R.F., Štípská, P., Li, P.F., Zhang, J., Chopin, F., Wang, S., Xia, X.P., Xiao, W.J., 2019. Structural and Geochronological Constraints on Devonian Suprasubduction Tectonic Switching and Permian Collisional Dynamics in the Chinese Altai, Central Asia. Tectonics 38, 253-280.

Jiang, Y.D., Schulmann, K., Sun, M., Štípská, P., Guy, A., Janoušek, V., Lexa, O., Yuan, C., 2016. Anatexis of accretionary wedge, Pacific-type magmatism, and formation of vertically stratified continental crust in the Altai Orogenic Belt. Tectonics 35, 3095-3118.

Jiang, Y.D., Štípská, P., Sun, M., Schulmann, K., Zhang, J., Wu, Q.H., Long, X.P., Yuan, C., Racek, M., Zhao, G.C., Xiao, W.J., 2015. Juxtaposition of barrovian and migmatite domains in the chinese altai: A result of crustal thickening followed by doming of partially molten lower crust. Journal of Metamorphic Geology 33, 45-70.

Johnson, C.L., Amory, J.A., Graham, S.A., Lamb, M.A., Badarch, G., Affolter, M., 2008. Accretionary tectonics and sedimentation during late Paleozoic arc collision, China-Mongolia border region, in: A. Draut, P.C., and D. Scholl (Ed.), Formation and applications of the sedimentary record in arc collision zones, pp. 363-390.

Jones, D.L., Howell, D.G., Coney, P.J., Monger, J.W.H., 1983. Recognition, character, and analysis of tectonostratigraphic terranes in western North America. Accretion tectonics in the circum-Pacific regions. Proc. seminar, 1981, Tomakomai, 21-35.

Jung, S., Masberg, P., Mihm, D., Hoernes, S., 2009. Partial melting of diverse crustal sources - constraints from Sr-Nd-O isotope compositions of quartz diorite-granodiorite-leucogranite associations (Kaoko Belt, Namibia). Lithos 111, 236-251.

Käufl, J. S., A. V. Grayver, M. J. Comeau, A. V. Kuvshinov, M. Becken, J. Kamm, E. Batmagnai, and S. Demberel, 2020. Magnetotelluric multiscale 3-D inversion reveals crustal and upper mantle structure beneath the Hangai and Gobi-Altai region in Mongolia, Geophysical Journal International, 221(2), 1002-1028.

Khomentovsky, V.V., Gibsher, A.S., 1996. The Neoproterozoic–lower Cambrian in northern Govi-Altay, western Mongolia: regional setting, lithostratigraphy and biostratigraphy. Geological Magazine 133, 371-390.

Kovalenko, V.I., Yarmoluyk, V.V., Sal'nikova, E.B., Kozlovsky, A.M., Kotov, A.B., Kovach, V.P., Savatenkov, V.M., Vladykin, N.V., Ponomarchuk, V.A., 2006. Geology, geochronology, and geodynamics of the Khan Bogd alkali granite pluton in southern Mongolia. Geotectonics 40, 450-466.

Kovalenko, V.I., Yarmolyuk, V.V., Kovach, V.P., Kotov, A.B., Kozakov, I.K., Salnikova, E.B., Larin, A.M., 2004. Isotope provinces, mechanisms of generation and sources of the continental crust in the Central Asian mobile belt: geological and isotopic evidence. Journal of Asian Earth Sciences 23, 605-627.

Kozakov, I.K., Sal'nikova, E.B., Khain, E.V., Kovach, V.P., Berezhnaya, N.G., Yakovleva, S.Z., Plotkina, Y.V., 2002. Early Caledonian crystalline rocks of the Lake Zone in Mongolia: formation history and tectonic settings as deduced from U–Pb and Sm–Nd datings. Geotectonics 36, 156–166.

Kröner, A., Kovach, V., Belousova, E., Hegner, E., Armstrong, R., Dolgopolova, A., Seltmann, R., Alexeiev, D.V., Hoffmann, J.E., Wong, J., Sun, M., Cai, K., Wang, T., Tong, Y., Wilde, S.A., Degtyarev, K.E., Rytsk, E., 2014. Reassessment of continental growth during the accretionary history of the Central Asian Orogenic Belt. Gondwana Research 25, 103-125.

Kröner, A., Lehmann, J., Schulmann, K., Demoux, A., Lexa, O., Tomurhuu, D., Štípská, P., Otgonbator, D., Liu, D.Y., Wingate, M.T.D., 2010. Lithostratigraphic and geochronological constraints on the evolution of the Central Asian Orogenic Belt in SW Mongolia: Early Paleozoic rifting followed by late Paleozoic accretion. American Journal of Science 310, 523-574.

Krýza, O., Lexa, O., Schulmann, K., Guy, A., Gapais, D., Cosgrove, J. and Xiao, W., (submitted). Oroclinal buckling and associated lithospheric-scale material flow - insights from physical modelling: implication for the Mongol-Hingan orocline.

Lamb, M.A., Badarch, G., 2001. Paleozoic sedimentary basins and volcanic arc systems of southern Mongolia: New geochemical and petrographic constraints, in: Hendrix, M.S., Davis, G.A. (Eds.), Paleozoic and Mesozoic Tectonic Evolution of Central and Eastern Asia: From Continental Assembly to Intracontinental Deformation. Memoir of the Geological Society of America, pp. 117-149.

Lamb, M.A., Hanson, A.D., Graham, S.A., Badarch, G., Webb, L.E., 1999. Left-lateral sense offset of Upper Proterozoic to Paleozoic features across the Gobi Onon, Tost, and Zuunbayan faults in southern Mongolia and implications for other central Asian faults. Earth and Planetary Science Letters 173, 183-194.

Lehmann, J., Schulmann, K., Lexa, O., Corsini, M., Kröner, A., Štípská, P., Tomurhuu, D., Otgonbator, D., 2010. Structural constraints on the evolution of the Central Asian Orogenic Belt in SW Mongolia. American Journal of Science 310, 575-628.

Lehmann, J., Schulmann, K., Lexa, O., Závada, P., Štípská, P., Hasalová, P., Belyanin, G., Corsini, M., 2017. Detachment folding of partially molten crust in accretionary orogens: A new magma-enhanced vertical mass and heat transfer mechanism. Lithosphere 9, 889-909.

Levashova, N.M., Gibsher, A.S., Meert, J.G., 2011. Precambrian microcontinents of the Ural-Mongolian Belt: New paleomagnetic and geochronological data. Geotectonics 45, 51-70.

Li, D., He, D., Tang, Y., 2016a. Reconstructing multiple arc-basin systems in the Altai-Junggar area (NW China): Implications for the architecture and evolution of the western Central Asian Orogenic Belt. Journal of Asian Earth Sciences 121, 84-107.

Li, P., Sun, M., Rosenbaum, G., Jiang, Y., Cai, K., 2016b. Structural evolution of zonal metamorphic sequences in the southern Chinese Altai and relationships to Permian transpressional tectonics in the Central Asian Orogenic Belt. Tectonophysics 693, 277-289.

Li, P., Sun, M., Rosenbaum, G., Jourdan, F., Li, S., Cai, K., 2017. Late Paleozoic closure of the Ob-Zaisan ocean along the Irtysh shear zone (NW China): Implications for arc amalgamation and oroclinal bending in the central Asian orogenic belt. Bulletin of the Geological Society of America 129, 547-569.

Liu, W., Liu, X.-J., Liu, L.-J., 2013. Underplating generated A- and I-type granitoids of the East Junggar from the lower and the upper oceanic crust with mixing of mafic magma: Insights from integrated zircon U–Pb ages, petrography, geochemistry and Nd–Sr–Hf isotopes. Lithos 179, 293-319.

Luo, J., Xiao, W., Wakabayashi, J., Han, C., Zhang, J.e., Wan, B., Ao, S., Zhang, Z., Tian, Z., Song, D., Chen, Y., 2017. The Zhaheba ophiolite complex in Eastern Junggar (NW China): Long lived supra-subduction zone ocean crust formation and its implications for the tectonic evolution in southern Altaids. Gondwana Research 43, 17-40.

Markova, N.G., 1975. Stratigraphy of the early and Middle Paleozoic of Western Mongolia. Moscow Nauka Press.

Martínez-Catalán, J.R., 2012. The Central Iberian arc, an orocline centered in the Iberian Massif and some implications for the Variscan belt. International Journal of Earth Sciences 101, 1299-1314.

Maus, S., Barckhausen, U., Berkenbosch, H., Bournas, N., Brozena, J., Childers, V., Dostaler, F., Fairhead, J.D., Finn, C., von Frese, R.R.B., Gaina, C., Golynsky, S., Kucks, R., Lühr, H., Milligan, P., Mogren, S., Müller, R.D., Olesen, O., Pilkington, M., Saltus, R., Schreckenberger, B., Thébault, E., Caratori Tontini, F., 2009. EMAG2: A 2–arc min resolution Earth Magnetic Anomaly Grid compiled from satellite, airborne, and marine magnetic measurements. Geochemistry, Geophysics, Geosystems 10, 1-12.

Meng, Q.-R., 2003. What drove late Mesozoic extension of the northern China–Mongolia tract? Tectonophysics 369, 155-174.

Miller, H.G., Singh, V., 1994. Potential field tilt—a new concept for location of potential field sources. Journal of Applied Geophysics 32, 213-217.

Molnar, P., Tapponnier, P., 1975. Cenozoic Tectonics of Asia: Effects of a Continental Collision. Features of recent continental tectonics in Asia can be interpreted as results of the India-Eurasia collision 189, 419-426.

Mordvinova, V.V., Artemyev, A.A., 2010. Three-dimensional shear velocity structure of lithosphere in the southern Baikal rift system and its surroundings. Russian Geology and Geophysics 51, 694-707.

Mordvinova, V.V., Deschamps, A., Dugarmaa, T., Deverchére, J., Ulziibat, M., Sankov, V.A., Artemyev, A.A., Perrot, J., 2007. Velocity structure of the lithosphere on the 2003 Mongolian-Baikal transect from SV waves. Izvestiya, Physics of the Solid Earth 43, 119-129.

Mossakovsky, A.A., Ruzhentsev, S.V., Samygin, S.G., Kheraskova, T.N., 1993. Central Asian fold belt geodynamic evolution and formation history Geotectonics 27, 29.

Nabighian, M.N., Ander, M., Grauch, V., Hansen, R., LaFehr, T., Li, Y., Pearson, W., Peirce, J., Phillips, J., Ruder, M., 2005b. Historical development of the gravity method in exploration. Geophysics 70, 63ND-89ND.

Nabighian, M.N., Grauch, V.J.S., Hansen, R.O., LaFehr, T.R., Li, Y., Peirce, J.W., Phillips, J.D., Ruder, M.E., 2005a. The historical development of the magnetic method in exploration. GEOPHYSICS 70, 33ND-61ND.

Nguyen, H., Hanžl, P., Janoušek, V., Schulmann, K., Ulrich, M., Jiang, Y., Lexa, O., Altanbaatar, B., Deiller, P., 2018. Geochemistry and geochronology of Mississippian volcanic rocks from SW Mongolia: Implications for terrane subdivision and magmatic arc activity in the Trans-Altai Zone. Journal of Asian Earth Sciences 164, 322-343.

Nikishin, A.M., Cloetingh, S., Lobkovsky, L.I., Burov, E.B., Lankreijer, A.C., 1993. Continental lithosphere folding in Central Asia (part I): Constraints from geological observations. Tectonophysics 226, 59-72.

Novikov, I.S., 2013. Reconstructing the stages of orogeny around the Junggar basin from the lithostratigraphy of Late Paleozoic, Mesozoic, and Cenozoic sediments. Russian Geology and Geophysics 54, 138-152.

Parfenov, L.M., Khanchuk, A.I., Badarch, G., Miller, R.J., Naumova, V.V., Nokleberg, W.J., Ogasawara, M., Prokopiev, A.V., Yan, H., 2003. Preliminary Northeast Asia Geodynamics Map. U.S. Geological Survey Open-File Report 03-205.

Pavlis, N.K., Holmes, S.A., Kenyon, S.C., Factor, J.K., 2012. The development and evaluation of the Earth Gravitational Model 2008 (EGM2008). Journal of Geophysical Research: Solid Earth 117, 1-38.

Petit, C., Déverchère, J., 2006. Structure and evolution of the Baikal rift: A synthesis. Geochemistry, Geophysics, Geosystems 7.

Petit, C., Déverchère, J., Calais, E., San'kov, V., Fairhead, D., 2002. Deep structure and mechanical behavior of the lithosphere in the Hangai-Hövsgöl region, Mongolia. New constraints from gravity modeling. Earth and Planetary Science Letters 197, 133-149.

Petit, C., Tiberi, C., Deschamps, A., Déverchère, J., 2008. Teleseismic traveltimes, topography and the lithospheric structure across central Mongolia. Geophysical Research Letters 35.

Phillips, J.D., 2001. Designing matched bandpass and azimuthal filters for the separation of potential-field anomalies by source region and source type, Australian Society of Exploration Geophysicists, 15th Geophysical Conference and Exhibition, Brisbane.

Rauzer, A.A., 1987. Geological Map 1:200,000 Open file report 4186: Geological Funds of Mongolia: Ulaanbaatar, Mongolia (in Russian), p. 769.

Ren, J., Tamaki, K., Li, S., Junxia, Z., 2002. Late Mesozoic and Cenozoic rifting and its dynamic setting in Eastern China and adjacent areas. Tectonophysics 344, 175-205.

Roberts, M.P., Clemens, J.D., 1993. Origin of high-potassium, calc-alkaline, I-type granitoids. Geology 21, 825-828.

Rojas-Agramonte, Y., Kröner, A., Demoux, A., Xia, X., Wang, W., Donskaya, T., Liu, D., Sun, M., 2011. Detrital and xenocrystic zircon ages from Neoproterozoic to Palaeozoic arc terranes of Mongolia: Significance for the origin of crustal fragments in the Central Asian Orogenic Belt. Gondwana Research 19, 751-763.

Rudnick, R.L., Fountain, D.M., 1995. Nature and composition of the continental crust: A lower crustal perspective. Reviews of Geophysics 33, 267-309.

Ruzhentsev, S.V., Badarch, G., Voznesenskaya, T.A., 1985. Tectonics of the Trans-Altai zone of Mongolia (Gurvansaykhan and Dzolen ranges). Geotectonics 19, 276-284.

Ruzhentsev, S.V., Pospelov, I., Badarch, G., 1992. The Inner-Mongolia ophiolitic sutures. Doklady Akademii Nauk SSSR 322, 953-958.

Saltus, R.W., Blakely, R.J., 2011. Unique geologic insights from "non-unique" gravity and magnetic interpretation. GSA Today 21, 8.

Scherer, E., Münker, C., Mezger, K., 2001. Calibration of the lutetium-hafnium clock. Science 293, 683-687.

Schulmann, K., Paterson, S., 2011. Geodynamics: Asian continental growth. Nature Geoscience 4, 827-829.

Şengör, A.M.C., Natal'in, B.A., Burtman, V.S., 1993. Evolution of the Altaid tectonic collage and Paleozoic crustal growth in Eurasia. Nature 364, 299-307.

Shen, X., Zhang, H., Wang, Q., Wyman, D.A., Yang, Y., 2011. Late Devonian–Early Permian A-type granites in the southern Altay Range, Northwest China: Petrogenesis and implications for tectonic setting of "A2-type" granites. Journal of Asian Earth Sciences 42, 986-1007.

Smithson, S.B., 1971. Densities of metamorphic rocks. Geophysics 36, 690-694.

Soejono, I., Čáp, P., Míková, J., Janoušek, V., Buriánek, D., Schulmann, K., 2018. Early Palaeozoic sedimentary record and provenance of flysch sequences in the Hovd Zone (western Mongolia): Implications for the geodynamic evolution of the Altai accretionary wedge system. Gondwana Research 64, 163-183.

Spector, A., Grant, F.S., 1970. Statistical models for interpreting magnetic data. Geophysics 35, 293-302.

Stewart, J.R., Betts, P.G., 2010. Implications for Proterozoic plate margin evolution from geophysical analysis and crustal-scale modeling within the western Gawler Craton, Australia. Tectonophysics 483, 151-177.

Štípská, P., Schulmann, K., Lehmann, J., Corsini, M., Lexa, O., Tomurhuu, D., 2010. Early Cambrian eclogites in SW Mongolia: Evidence that the Palaeo-Asian Ocean suture extends further east than expected. Journal of Metamorphic Geology 28, 915-936.

Sun, M., Yuan, C., Xiao, W., Long, X., Xia, X., Zhao, G., Lin, S., Wu, F., Kröner, A., 2008. Zircon U-Pb and Hf isotopic study of gneissic rocks from the Chinese Altai: Progressive accretionary history in the early to middle Palaeozoic. Chemical Geology 247, 352.

Syberg, F.J.R., 1972. A fourier method for the regional-residual problem of potential fields. Geophysical Prospecting 20, 47-75.

Telford, W.M., Geldart, L. P., Sheriff, R. E., 1990. Applied Geophysics (2nd Edition). Cambridge University Press.

Teng, J., Zhang, Z., Zhang, X., Wang, C., Gao, R., Yang, B., Qiao, Y., Deng, Y., 2013. Investigation of the Moho discontinuity beneath the Chinese mainland using deep seismic sounding profiles. Tectonophysics 609, 202-216.

Tiberi, C., Deschamps, A., Déverchère, J., Petit, C., Perrot, J., Appriou, D., Mordvinova, V., Dugaarma, T., Ulzibaat, M., Artemiev, A.A., 2008. Asthenospheric imprints on the lithosphere in Central Mongolia and Southern Siberia from a joint inversion of gravity and seismology (MOBAL experiment). Geophysical Journal International 175, 1283-1297.

Tong, L., Xu, Y.G., Cawood, P.A., Zhou, X., Chen, Y., Liu, Z., 2014. Anticlockwise P-T evolution at ~280 Ma recorded from ultrahigh-temperature metapelitic granulite in the Chinese Altai orogenic belt, a possible link with the Tarim mantle plume? Journal of Asian Earth Sciences 94, 1-11.

Tunini, L., Jiménez-Munt, I., Fernandez, M., Vergés, J., Villaseñor, A., Melchiorre, M., Afonso, J.C., 2016. Geophysical-petrological model of the crust and upper mantle in the India-Eurasia collision zone. Tectonics 35, 1642-1669.

Verduzco, B., Fairhead, J.D., Green, C.M., MacKenzie, C., 2004. New insights into magnetic derivatives for structural mapping. Leading Edge (Tulsa, OK) 23, 116-119.

Vishnevskaya, I., Letnikova, E., Pisareva, N., Proshenkin, A., 2015. Chapter 18 - Chemostratigraphy of Neoproterozoic Carbonate Deposits of the Tuva–Mongolian and Dzabkhan Continental Blocks: Constraints on the Age, Glaciation and Sedimentation, in: Ramkumar, M. (Ed.), Chemostratigraphy. Elsevier, Oxford, pp. 451-487.

Wang, J., Meng, X., Chen, Z., Liu, G., Zheng, Y., Wang, J., Zhang, S., Zhang, X., Zheng, W., 2015. Lithologic mapping test for gravity and magnetic anomalies: A case study of gravity–magnetic anomaly profile in the eastern segment of the China–Mongolia border. Journal of Applied Geophysics 117, 23-31.

Wang, T., Jahn, B.-M., Kovach, V.P., Tong, Y., Hong, D.-W., Han, B.-F., 2009. Nd–Sr isotopic mapping of the Chinese Altai and implications for continental growth in the Central Asian Orogenic Belt. Lithos 110, 359-372.

Wang, T., Tong, Y., Zhang, L., Li, S., Huang, H., Zhang, J., Guo, L., Yang, Q., Hong, D., Donskaya, T., Gladkochub, D., Tserendash, N., 2017. Phanerozoic granitoids in the central and eastern parts of Central Asia and their tectonic significance. Journal of Asian Earth Sciences 145, 368-392.

Wang, Y., Mooney, W.D., Yuan, X., Coleman, R.G., 2003. The crustal structure from the Altai Mountains to the Altyn Tagh fault, northwest China. Journal of Geophysical Research: Solid Earth 108, 1-16.

Webb, L.E., Johnson, C.L., 2006. Tertiary strike-slip faulting in southeastern Mongolia and implications for Asian tectonics. Earth and Planetary Science Letters 241, 323-335.

Wellman, P., 1988. Development of the Australian Proterozoic crust as inferred from gravity and magnetic anomalies. Precambrian Research 40-1, 89-100.

Wilhem, C., Windley, B.F., Stampfli, G.M., 2012. The Altaids of Central Asia: A tectonic and evolutionary innovative review. Earth-Science Reviews 113, 303-341.

Windley, B.F., Alexeiev, D., Xiao, W., Kröner, A., Badarch, G., 2007. Tectonic models for accretion of the Central Asian Orogenic Belt. Journal of the Geological Society 164, 31-47.

Windley, B.F., Kröner, A., Guo, J., Qu, G., Li, Y., Zhang, C., 2002. Neoproterozoic to Paleozoic Geology of the Altai Orogen, NW China: New Zircon Age Data and Tectonic Evolution. The Journal of Geology 110, 719-737.

Xiao, W., Huang, B., Han, C., Sun, S., Li, J., 2010. A review of the western part of the Altaids: A key to understanding the architecture of accretionary orogens. Gondwana Research 18, 253-273.

Xiao, W., Windley, B.F., Badarch, G., Sun, S., Li, J., Qin, K., Wang, Z., 2004. Paleozoic accretionary and convergent tectonics of the southern Altaids: Implications for the growth of Central Asia. Journal of the Geological Society 161, 339.

Xiao, W., Windley, B.F., Han, C., Liu, W., Wan, B., Zhang, J., Ao, S., Zhang, Z., Song, D., 2018. Late Paleozoic to early Triassic multiple roll-back and oroclinal bending of the Mongolia collage in Central Asia. Earth-Science Reviews 186, 94-128.

Xiao, W., Windley, B.F., Sun, S., Li, J., Huang, B., Han, C., Yuan, C., Sun, M., Chen, H., 2015. A tale of amalgamation of three permo-triassic collage systems in central Asia: Oroclines, sutures, and terminal accretion, Annual Review of Earth and Planetary Sciences, pp. 477-507.

Xiao, W.J., Windley, B.F., Yuan, C., Sun, M., Han, C.M., Lin, S.F., Chen, H.L., Yan, Q.R., Liu, D.Y., Qin, K.Z., Li, J.L., Sun, S., 2009. Paleozoic multiple subduction-accretion processes of the southern Altaids. American Journal of Science 309, 221-270.

Xiong, S., Yang, H., Ding, Y., Li, Z., Li, W., 2016. Distribution of igneous rocks in China revealed by aeromagnetic data. Journal of Asian Earth Sciences 129, 231-242.

Yang, T.N., Li, J.Y., Zhang, J., Hou, K.J., 2011. The Altai-Mongolia terrane in the Central Asian Orogenic Belt (CAOB): A peri-Gondwana one? Evidence from zircon U–Pb, Hf isotopes and REE abundance. Precambrian Research 187, 79-98.

Yarmolyuk, V.V., Kovach, V.P., Kozakov, I.K., Kozlovsky, A.M., Kotov, A.B., Rytsk, E.Y., 2012. Mechanisms of continental crust formation in the Central Asian Foldbelt. Geotectonics 46, 251-272.

Yarmolyuk, V.V., Kovalenko, V.I., Kozlovsky, A.M., Kovach, V.P., Sal'Nikova, E.B., Kovalenko, D.V., Kotov, A.B., Kudryashova, E.A., Lebedev, V.I., Eenzhin, G., 2008. Crust-Building Processes in the Hercynides of the Central Asian Foldbelt. Petrology 16, 679-709.

Yarmolyuk, V.V., Kuzmin, M.I., Kozlovsky, A.M., 2013. Late paleozoic-Early Mesozoic within-plate magmatism in North Asia: Traps, rifts, giant batholiths, and the geodynamics of their origin. Petrology 21, 101-126.

Yushan, Y., Yuanyuan, L., Tianyou, L., 2012. Gravity and magnetic investigation on the distribution of volcanic rocks in the Qinggelidi area, north- eastern Junggar Basin (north- west China). Geophysical Prospecting 60, 539-554.

Zhang, J., Sun, M., Schulmann, K., Zhao, G., Wu, Q., Jiang, Y., Guy, A., Wang, Y., 2015. Distinct deformational history of two contrasting tectonic domains in the Chinese Altai: Their significance in understanding accretionary orogenic process. Journal of Structural Geology 73, 64-82.

Zhang, J., Wang, T., Tong, Y., Zhang, Z., Song, P., Zhang, L., Huang, H., Guo, L., Hou, Z., 2017. Tracking deep ancient crustal components by xenocrystic/inherited zircons of Palaeozoic felsic igneous rocks from the Altai–East Junggar terrane and adjacent regions, western Central Asian Orogenic Belt and its tectonic significance. International Geology Review 59, 2021-2040.

Zhang, P.-Z., Shen, Z., Wang, M., Gan, W., Bürgmann, R., Molnar, P., Wang, Q., Niu, Z., Sun, J., Wu, J., Hanrong, S., Xinzhao, Y., 2004. Continuous deformation of the Tibetan Plateau from global positioning system data. Geology 32, 809-812.

Zhang, Z., Zhang, G., Deng, Y., Santosh, M., Teng, J., 2014. Geophysical transect across the North China Craton: A perspective on the interaction between Tibetan eastward escape and Pacific westward flow. Gondwana Research 26, 311-322.

Zhao, J., Liu, G., Lu, Z., Zhang, X., Zhao, G., 2003. Lithospheric structure and dynamic processes of the Tianshan orogenic belt and the Junggar basin. Tectonophysics 376, 199-239.

Zonenshain L.P., K.M.I., Natapov L.M, 1990. Geology of the USSR: a plate tectonic synthesis.

Zonenshain, L.P., 1973. The evolution of Central Asiatic geosynclines through sea-floor spreading. Tectonophysics 19, 213-232.

Zonenshain, L.P., Kuzmin, M.I., 1978. Khantaishir ophiolite complex in western Mongolia and ophiolite problem. Geotectonics 1, 19-42.

Zorin, Y.A., Belichenko, V.G., Turutanov, E.K., Kozhevnikov, V.M., Ruzhentsev, S.V., Dergunov, A.B., Filippova, I.B., Tomurtogoo, O., Arvisbaatar, N., Bayasgalan, T., Biambaa, C., Khosbayar, P., 1993. The South Siberia-Central Mongolia transect. Tectonophysics 225, 361.

Zorin, Y.A., Belichenko, V.G., Turutanov, E.K., Mazukabzov, A.M., Sklyarov, E.V., Mordvinova, V.V., 1995. The East Siberia Transect. International Geology Review 37, 154-175.

AUTHORS OF THE REVIEW



Alexandra Guy is a researcher in geophysics and geology at the Centre for Lithospheric Research hosted by the Czech Geological Survey in Prague, Czech Republic. She studied geophysics and geology at the University of Strasbourg and Ecole et Observatoire des Sciences de la Terre (EOST) where she obtained her Ph.D. degree in 2012. From 2013 until now, she works as a researcher in Prague. Her main research interests are the geophysical and geological characterization of accretionary and collisional orogenic systems using potential field analyses and modelling combined with structural and tectonic analyses. She works on projects related to the Central Asian Orogenic Belt, the Bohemian Massif and East Antarctica. She is a member of the editorial board of the Journal of GEOsciences.



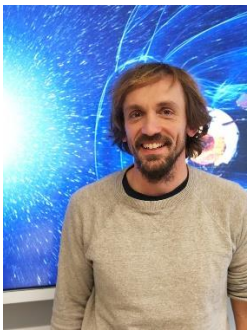
Karel Schulmann is an exceptional class Professor of geology at the University of Strasbourg, France and head of Centre for Lithospheric Research at the Czech Geological Survey, Czech Republic. He studied geology at Charles University in Prague, Czech Republic where he obtained his Ph.D. degree in 1987 and habilitation in 1991. From 2001 until

2004, he worked as a professor and the head of the Department of Petrology & Structural Geology, Charles University, Prague, Czech Republic. From 2004 until now, he is a professor at the University of Strasbourg (former University Louis Pasteur), France. Since 2012's he joined also the Czech Geological Survey, gue, Czech Republicwhere he acts as the director of a research center and where he was appointed a national research grant for the study of the accretionary and collisional Paleozoic systems. He is an editor of International Journal of Earth Sciences, Journal of the Geological Society of London and associated editor of Tectonics and Terra Nova. He is a member of an Editorial Review Boards of several national journals (Slovakia, Russia, Czech Republic, France). His main research interests are geodynamics, tectonics and structural geology of accretionary and collisional orogenic belts.



Igor Soejono is a research geologist at the Department of Regional Geology of Crystalline Complexes, Czech Geological Survey, Czech Republic. He studied geology at Charles University in Prague, Czech Republic where he obtained M.Sc. degree in 2004 and Ph.D. degree in 2019. He works in the Czech Geological Survey since 2005. His main scientific focus is geotectonics studied by the combination of geological mapping with structural analysis, geochemistry and geochronology with particular interest in the Bohemian Massif and the Central Asian Orogenic Belt.

Journal Pre-proof



Nils Holzrichter is a postdoctoral researcher at the Institute of Geosciences of Kiel University in Germany. He studied geophysics at Kiel University where he received his Ph.D. degree in 2013. After that he continued his work as a postdoctoral researcher in the working group satellite and aerogeophysics. He is an expert in lithospheric modelling with satellite and terrestrial potential fields. This includes forward modelling and inversion, applied interpretation techniques of potential fields and thorough knowledge of several processing techniques. He works on several projects related to applications for interpreting and constraining the structure of the Earth on a global and local scale with potential fields.



Ondrej Lexa is an associate professor of structural geology and geotectonics at the Charles University in Prague. He received M.S. degree in geology from Comenius University in Bratislava (1995) and Ph.D. in geosciences from Charles University (2003). He also worked as a Post Doc at University in Strasbourg. He has more than 25 years of field experience from West Carpathians, Bohemian Massif and Mongolian Altay. His research interests involve quantitative analyses of microstructural to tectonic-scale deformations, numerical modelling of deformational processes and structural analysis of polyphase deformational patterns.

Journal Pre-proof



Marc Munschy is professor of geophysics at the University of Strasbourg, France. He studied geophysics at University of Strasbourg and School of Engineering Geophysics and he obtained his Ph.D. degree in 1987 and habilitation in 1994. Since 1987, he is working as a professor at the University of Strasbourg (former University Louis Pasteur). His main research interest is potential field methods (gravity and magnetic) applied to Earth sciences, naval ship magnetism and unexploded ordnance and pipeline detection. His recent research has focused on the theory of potential field methods using complex algebra and mapping and characterizing subsurface geology using drones. He also served as an expert for the quality control and interpretation of airborne geophysical surveys (World Bank and Democratic Republic of Congo, 2017-2019).

Declaration of interests

☒ The authors declare that they have no known competing financial interests or personal relationships that could have appeared to influence the work reported in this paper.

☐The authors declare the following financial interests/personal relationships which may be considered as potential competing interests:

Journal Pre-proof

HIGHLIGHTS (85 CHARACTERS INCLUDING SPACES):

- Potential field data do not correlate with geologically defined terranes in the CAOB
- Geophysics determines two orthogonal supra-crustal Paleozoic and Mesozoic fabrics
- Geophysics and isotopic mapping identify a homogeneous lower crust

Journal Pre-proof